INVESTIGATION OF RETINAL PIGMENT EPITHELIUM REGENERATION IN WOUND HEALING MICE

By

HUIMING XIA

A DISSERTATION PRESENTED TO THE GRADUATE SCHOOL
OF THE UNIVERSITY OF FLORIDA IN PARTIAL FULFILLMENT
OF THE REQUIREMENTS FOR THE DEGREE OF
DOCTOR OF PHILOSOPHY

UNIVERSITY OF FLORIDA

2012

To my beloved wife Luning Zhuang

ACKNOWLEDGMENTS

I would first like to thank my mentor, Dr. Edward Scott, for the excellent training and opportunities I received in his lab. He taught me patiently in all the aspect of both life and science. Due to his mentorship I have gained invaluable knowledge on how to organize my research. I would also like to thank the all the members of my committee, Dr. Alfred Lewin, Dr. Edward Chan and Dr. Maria Grant, for their time, energy, effort and guidance in my research for the past several years. Your invaluable suggestions are critical for my project. I am deeply grateful to my partner Dr. Mark Krebs for his unselfish guidance and help on the project. His rigorousness, passion on science let me realized what qualities a scientific researcher should have. Without his help, my project cannot proceed so confluently. I would also like to thank Dr. Liya Pi for the encouragement, for the discussion and suggestions on my research. In addition, I want to thank Gary Brown for his mouse expertise, computer and network support. I must thank Li Lin and Dustin Hart for all the support on the reagents and facilities. My deepest thanks also are extended to my fellow graduate students, Seung-Bum Kim, Anitha Shenoy and David Lopez. The time I spend in the lab with you I will forever cherish. I would like to thank Hong Li for her help on the plastic sectioning. I would also like to thank the staffs of the core facilities at UF, Marda Jorgensen, Neal Benson and Doug Smith for their support and expertise.

Finally, I would like to thank my family members, my father in the heaven, my mother, my father and mother in law and my wife Luning. Your unconditioned love is my motivation and strength.

TABLE OF CONTENTS

page

LIST OF FIGURES

LIST OF ABBREVIATIONS

AMD	Age Related Macular Degeneration
CDK	Cyclin-dependent kinase
CNV	Choroidal neovascularization
Brdu	Bromodeoxyuridine
ECM	Extracellular matrix
ERG	Electroretinography
FACS	Fluorescence Activated Cell Sorting
GFP	Green Fluorescent Protein
HSC	Hematopoietic stem cells
K.O.	Knockout
FBS	Fetal Bovine Serum
TGF-β	Transforming growth factor β
MMP	Matrix metalloproteinase
MRL/MpJ	Murphy Roths Large derived by the Murphy (Mp) group of the Jackson Laboratory
ONL	Outer nuclear layer
ROS	Reactive oxygen species
RPE	Retinal Pigment Epithelium
sFRP2	Secreted frizzled-related protein 2
PBS	Phosphate Buffered Saline
PFA	Paraformaldehyde
P.I.	Post Injection
PLK1	Polo-like kinase 1

Abstract of Dissertation Presented to the Graduate School
of the University of Florida in Partial Fulfillment of the
Requirements for the Degree of Doctor of Philosophy

INVESTIGATION OF RETINAL PIGMENT EPITHELIUM REGENERATION IN WOUND HEALING MICE

By

Huiming Xia

May 2012

Chair: Edward William Scott
Major: Medical Sciences – Molecular Genetics and Microbiology

Regenerative medicine holds the promise of restoring cells and tissues that are destroyed in human disease. However, development of this approach in the eye has been limited by a lack of mammalian models that show robust regeneration of ocular tissue. Here, the potential of retinal pigment epithelium (RPE) regeneration ability in wound healing strains and possible mechanisms were investigated. We test whether MRL/MpJ mice, which exhibit enhanced wound healing, can efficiently regenerate the RPE after an injury that mimics the loss of this tissue in age-related macular degeneration. The RPE of MRL/MpJ and control AKR/J mice was injured by injection of sodium iodate at 20 mg/kg body weight, which titration studies indicated was optimal for highlighting strain differences in the response to injury. Five days after injection, electroretinography (ERG) of both strains revealed equivalent and reduced retinal responses. At one and two months post-injection, retinal responses were restored in MRL/MpJ but not AKR/J mice. Brightfield and fluorescence microscopy of eyecup cryosections indicated an initial central loss of RPE cells in MRL/MpJ and AKR/J mice, with preservation of peripheral RPE. Phalloidin staining of posterior eye wholemounts

confirmed this pattern of RPE loss, and revealed a transition region characterized by RPE cell shedding and restructuring in both strains, suggesting a similar initial response to injury. At one month post-injection, central RPE cells, RPE65 immunostaining and phalloidin staining were restored in MRL/MpJ but not AKR/J mice. BrdU incorporation was observed throughout the RPE of MRL/MpJ but not AKR/J mice one month following sodium iodate treatment, consistent with RPE proliferation. These findings provide evidence for a dramatic regeneration of the RPE after injury in MRL/MpJ mice that supports full recovery of retinal function, which has not been observed previously in mammalian eyes. In order to elude the genetic background uncertainty of MRL/MpJ mice, B6.129S6(Cg)-Cdkn1atm1Led/J mice (p21 K.O.), which has a single gene knockout and has similar wound healing ability, was introduced in later study. To investigate possible underlying regeneration mechanism, cross bone marrow transplantation was conducted among wound healing and non-wound healing strains. After sodium iodate injury, C57BL/6 transplanted with p21 K.O. bone marrow cells displayed regeneration ability similar to the donor, while p21 K.O. host transplanted with C57BL/6 chimera shown limited regeneration ability. This result indicated that the bone marrow derived cells may contribute more than the micro-environment. Our study should prove useful for understanding molecular mechanisms that underly regeneration, and for identifying factors that promote RPE regeneration in age-related macular degeneration and related diseases.

CHAPTER 1
BACKGROUND AND SIGNIFICANCE

AMD and RPE

Introduction to AMD

The Age-related-macular degeneration (AMD) is an incurable eye disorder. It is the leading cause of the blindness of the western community including Australia and affects more than 10 million patients in U.S. alone, causing devastating impact on quality of life in a significant fraction of the elderly population worldwide (1). The number of affected population is forecasted to reach 14.6 million in 2050 (2). Study the potential treatment of this disease will benefit dramatically to the community.

In general, AMD is the multifactorial disease of aging. Many risk factors, including environmental, life habits, like smoking, and genetic factors, will alter an individual's susceptibility. Aging changes in the RPE–Bruch membrane-choriocapillaris complex are highly associated with AMD. The prevalence of this disease increases significantly with age (3-5).

Pathobiology of AMD

AMD is characterized by the degenerative changes in the macula, the central region of the retina bearing the highest concentration of cones and responsible for central vision and visual acuity (6). Clinically and histologically, it can be divided into atrophic AMD (dry AMD) and exudative AMD (wet AMD). Dry AMD is featured by outer RPE atrophy and subjacent choriocapillaris degeneration representing an early form of AMD. Wet AMD is characterized by choroidal neovascularizton (CNV) followed by subsequent clinical phenotype including hemorrhage, exudative retinal detachment,

disciform scarring, and retinal atrophy (7).The normal and pathological features of retina are illustrated in Figure 1-1, Figure 1-2 and Figure 1-3 (8).

AMD is a progressive disease with exudative AMD a more advanced and more damaging type. The pathological process is initiated by the aging changes in the RPE and choroicapillary which lead to the chronic inflammation. Extensive damage to RPE, choroid and the extra damage introduced by inflammation results in the abnormality of extracellular matrix (ECM), change of composition and permeability of Bruch's membrane. The diffusion of product wastes, hormones and nutrients through Bruch's membrane may stimulate the secretion of VEGF by RPE. The change of RPE-choriocapillaris behavior will ultimately leading to atrophy of the retina, RPE and CNV (7).

In the process, the accumulation of extracellular debris changes the and lead to the diffusion of product wastes, hormones and nutrients to RPE layer. In response to this metabolic distress, the RPE probably produce VEGF and basic fibroblast growth factors and stimulate CNV.

Drusen, the extracellular deposit of protein and lipid that accumulate beneath the RPE, is one of the distinct disease characteristics in AMD. Drusen composition and origin have been analyzed extensively in the hope of searching for the pathogenesis of AMD. It is believed that most of the drusen components are from RPE, neural retina, or choroidal cells but some are from extraocular sources. Many different types of molecules have been identified. Among them are amyloid β (Aβ), vitronectin, amyloid P, apolipoprotein E, as well as inflammatory mediators and complement components. This findings have led to the suggestion the association of AMD with atherosclerosis

(vitronectin, apolipoproteins B and E, complement and lipid), with inflammation (amyloid P component, C5 and α1-antitrypsin; vitronectin, apolipoprotien E and C5; C5, C5b9 and C3) and with cholesterol metabolism (cholesterol and its transporter, apoE) (7, 9, 10).

In this pathological process of AMD, dysfunction and eventual loss of the RPE is considered as critical step in AMD pathology. The abnormal changes in the RPE and choriocapillaris will finally lead to the atrophy of the retina, and change of RPE-choriocapillaris. These pathological changes will progressively lead to the CNV and severe damage to photoreceptor cells (7).

RPE Structure and Function

RPE layer is a monolayer of cuboidal cells which separates the photoreceptors and the choroid forming a part of the blood/retina barrier (11). With its specific apical tight junctions and asymmetrical distributed vectorial transport proteins, the RPE nourishes retinal visual cells by taking up nutrients such as glucose, retinol, and fatty acids from the blood and deliver to photoreceptors, and by exchanging ions, water, and metabolic end products with the circulating system. RPE cells also participate in vision function by absorbing light energy and working as reisomerize enzyme in vision cycle. As a result, the RPE layer is essential for maintaining retinal health and vision function (Figure 1-4) (12).

It is commonly believed that the RPE cells are terminally differentiated and will not proliferate or at most at very low rate (13). As a result, there is no restorative treatment for AMD, unless replenish source of RPE can be explored and utilized in clinical trials, to replace the damaged or loss of RPE cells in AMD patients.

Current Strategies for AMD Treatment

So far, many strategies and methods targeting different pathological procedure have been developed (Figure 1-5). Most of them are design to slow the pathological progression or alleviate the symptom. As a result, they cannot eventually reverse the pathological damage and recovery of normal physiological function of the retina. Regenerative approach is promising for the recovery of damaged or loss of unrenewable tissues.

Antioxidant Therapy

The macula is a location with high metabolic activity and RPE is therefore exposed to high levels of reactive oxygen species (ROS). Polymorphism of genes involved in controlling oxidative stress is found to be one of the risk factors of AMD (14). Accumulating evidence indicate that oxidative damage contributes to the pathogenesis of AMD by directly damage RPE, interfere impairs local complement inhibition and accelerate neovascularization (15-17). Age-Related Eye Disease Study (AREDS) results indicate that supplementing of high-dose antioxidants plus zinc significantly reduce the risk of advanced AMD and its associated vision loss (http://www.nei.nih.gov/amd/). This nutrient therapy is highly cost-effective (18). Antioxidant gene therapy may also provide an option for the long-term protection against damage and degeneration caused by oxidative stress (19, 20).

Suppressing Inflammation

Proteomic studies of the composition of drusen, as well as genetic association studies have revealed a connection between complement system and AMD (21). POT-4 and eculizumab are two drugs that work to interfere with the complement system and inhibit the activation of downstream cascade. POT-4 is an analogue of the small cyclic

synthetic peptide compstatin. By blocking the amplification of the complement response at central stage complement cascade, POT-4 act to inhibit downstream effector functions (22). Eculizumab is an anti- complement protein C5 mono antibody. By specific binding by eculizumab, the complement protein C5 evade the cleavage by C5 convertase and prevent the generation of C5b-9b [www.clinicaltrials.gov/ct2/show/NCT00935883]. Both drugs have been entered into the phase II clinical trials to test the effect on reduction on drusen volume and area of geographic atrophy.

Anti-neovascularization

The more debilitating and rapid progressive form of AMD is the exudative form, which is characterized by the choroidal neovascularization (CNV). Since 1970, laser was adopted to ablate CNV in the exudative AMD. Macular Photocoagulation Study reported that laser photocoagulation of CNV in exudative AMD reduced the risk of severe visual loss (23, 24). Administration of anti-angiogenesis agents, such as anti-VEGF drugs is usually utilized cooperatively with the laser surgery, aiming to inactivate vascular endothelial growth factor and inhibit CNV (25, 26). Two anti-VEGF agents, pegaptanib sodium and ranibizumab, have been approved in clinical trials and proved to be effective in preventing vision loss (27). Besides, genetic tools are investigated to be used as novel strategies for the silencing of VEGF gene expression (28-30).

Surgical Approaches

One surgical approach is to remove hemorrhagic choroidal neovascularization. It is reported that the patient group whose hemorrhage was surgically removed will have decreased chance of losing visual acuity (VA) compared to untreated group (31). This approach was later abandoned due to the low efficiency and replaced by the subretinal

injection of recombinant tissue plasminogen activator and 20%-SF6 gas. The possible mechanism is to liquefy and displace the hemorrhage clot. Complete displacement of submacular hemorrhage was achieved in as many as 50% of treated patients (32). The second, surgical approach is called Macular Translocation Surgery. The goal is to lift the macula away from underlying blood vessels and move it to a new, healthier location to restore central vision, in patients who are losing the last of their central vision to AMD. The macular function after RPE-choroid graft transplantation can be maintained up to 7 years with low rate of recurrence (33).

Regenerative Medicine and RPE Restoration in AMD

Regenerative Medicine

The motivating concept of regenerative medicine is that physically or functionally damaged cells, tissues, and organs might be restored in patients with severe injuries or chronic diseases (34). Inspiring examples include the regeneration of amputated limb (Figure 1-6), lesioned spinal cord, lens, jaws and tails in amphibian (35-38) and truncated heart in zebrafish (39). Regeneration is not limited to amphibians, regeneration of blood cells (40), antler (41), liver (42, 43) and digital tip (44) are common phenomena in high vertebrate including human. Using regenerative medicine as a therapy can be traced back to 1960 when whole bone marrow transplantation is used to treat leukemia. It is working towards treating lots of stubborn diseases, like heart disease (45-47).

Treatment of RPE Loss in AMD

AMD is one important disease target due to low efficacy of current treatment strategies and the fact that mammalian RPE is essentially non-renewable by itself (13, 48). Due to the critical functions RPE carrying during visual activities, without replenish

RPE, none of these treatments can fully restore the vision health. As a result, it is critical to develop a therapeutic approach, which can provide replacement source for the damage or loss of RPE in AMD to fully restore the normal vision function. Several regenerative approaches have been investigated, as discussed below.

An ex-vivo way is to introduce cultured RPE cells deriving from embryonic or induced pluripotent stem cells into the subretinal space. This approach show some efficacy but the application is limited by the immune rejection, a limited source of donor cells, and surgical complications as well as the lack of effect on halting disease progression (49, 50).

A second approach is to deliver bone marrow derived stem cells into the intra-vitreous or circulating system anticipated to working as a regeneration source for RPE replacement. Intriguing results have been reporting by other lab and ours identifying RPE cells transdifferentiated from bone marrow-derived cells in rodent models. Shortcoming of this approach is the efficiency, which is currently too low to be considered as a robust therapy (51-56).

Another untested strategy is to trigger reprogramming of resident stem cells or undamaged RPE cells to repopulate the damaged tissue, by local introducing regeneration chemically to wound site, as proposed in other organs(57).

The investigation of organisms with high regenerative capacity like MRL/MpJ mice is another promising direction for regenerative medicine. The rationale is to identify regenerative factors and then make modifications on the damaged locus so that it can recapitulate the regeneration in regenerative organisms.

Wound Healing and Regeneration

Wound Healing

Tissue repair or wound healing is an essential ability for survival allowing animals to escape danger and recover from injury. There are two kinds of tissue repair categories: scarring and scar-free healing. Fibrosis and scarring is the normal outcome of tissue repair seen in adult advanced vertebrates including mammals. Wound healing is composed of a series of sequential events. It begins from fibrin clot deposition, platelets aggregation, followed by inflammation, keratinocytes re-establishing, granulation tissue formation, remodeling and scar forming. Fetal wound repair, on the other hand, represents another category of tissue repair which was characterized by absent of scarring and fibrosis and by complete restoration of normal structure and function. This kind of regeneration only exists during the first third of human development (58, 59). It will be clinically attractive if non-scar wound healing be extended throughout life.

Wound healing is a complex process involving many factors. Among them, molecular signaling plays critical roles. The close association between TGF-β family member TGF-β1, TGF-β2, and TGF-β3 expression profile and the pattern of tissue repairing indicates that they are important mediators in wound signaling. It is indicated that low level of TGF-β1, TGF-β2 and high level of TGF-β3 will result in scar-free tissue repair, as seen in embryonic wounds healing. Inhibition of TGF-β1, TGF-β2 (60) and exogenous addition of TGF-β3 (61) were able to induce scar free tissue repair. Similarly, TGF-β family members were also found involved in amphibian limb, tail regeneration (62, 63). As a result, there seems to have some strong connection between TGF-β

family and proliferation and regeneration. Study or modification the expression profile of TGF-β1,2, and 3 may provide some clues on investigation of RPE regeneration.

MRL/MpJ Mice

The ability to regenerate damaged tissue and/or organs is seen in many non-mammalian species. This ability, however, disappears in most of advanced vertebrates which end up with scaring as mentioned above. A laboratory inbreeding strain, MRL/MpJ mice is among few examples of adult mammal regeneration, which has the ability to completely close 2 mm ear punch, a classic way of numbering mice colony. Upon ear punch injury, MRL mice regrow cartilage, skin, and hair follicles, which reminiscent of regeneration in amphibians (64).

The regeneration is not limited to the ear but also observed in other organs as well including heart (65), cornea (66), articular cartilage (67), and axon (68). The MRL mice strain was generated through the interbreeding among LG mouse, the AKR mouse, the C3H mouse and the C57BL/6 mouse. Crossbreeding experiments indicated that the regeneration process is a complex, mutagenic process involving 20 loci(69). It is also found that the regeneration is sexually dimorphic with female mice heal faster than the male. Studying of regeneration mechanism revealed an upregulation of Ki-67 expression in the early stage of injury and BrdU incorporation suggesting the involvement of cell division or differentiation (64). Recent evidence indicate the MRL mice have superior mesenchymal stem cell resulted from the inhibition of Wnt signaling by sFRP2 (70). Biochemistry study data discovered that a number of features of embryonic metabolism were found to be retained in adult MRL mice. Populations of cells that express the markers of embryonic stem cells are also found to be retained. Both of them are rare in mammals (71). Proteomic study by using tissue profiling matrix-

assisted laser desorption ionization (MALDI) mass spectrometry (MS) implicated the involvement of calcium-binding proteins calgranulin A and B, calgizzarin, and calmodulin in the wound healing procedure (72). Another key event during the regeneration is the destruction of the basal membrane, a process associated with matrix metalloproteinase (MMPs) and its inhibitor including TIMP. It is found that upon injury, the level of MMP-2 and MMP-9 was up regulated in the healing situation, indicative of creating a permissive environment for regeneration (63). These molecules are mostly expressed by inflammatory cells and brought to the site soon after wounding (64). Suggested by this as well as other evidence, the involvement of immune system in the response to regeneration is now become a hot crossover topic.

p21 Knockout Mice and Wound Healing

MRL/MpJ mouse is a hybrid strain of many ancestor strains. The difficulty of study the regeneration process in MRL/MpJ mice is that there so many regeneration loci, it would be impossible to make genetic modification on normal situation to make it regeneration like MRL/MpJ. This problem is bypassed by studying the regeneration of another strain, B6.129S6(Cg)-Cdkn1atm1Led/J, a strain that contains a mutation in a single gene. In this strain, a p21 (Cdkn1a), cyclin-dependent kinase inhibitor 1A is knocked out, and interestingly, the regeneration is enhanced (2). The regeneration is p53 independent indicating is it not involved in the p21/p53 pathway. Detailed mechanism still unclear but the single gene mutant regeneration strain is extremely useful to study and in turn to apply the regeneration mechanism in clinical trials in the future (69).

Stem Cell and Regeneration

The Definition and Function of Stem Cell

Stem cell is an indispensable component in the regeneration process. It is defined as a cell population capable of both self-renew and differentiation into at least one specified cell type. Stem cells are essential for the maintenance of normal function of tissue with high rate of cellular turnover and for the repair of injury in adults. There are two kinds of self-renewal pattern: symmetric and asymmetric self-renewal. In the symmetric self-renewal, both daughter cells retain stem cell property while in the asymmetric self-renewal, on daughter cell remain stem cell property and the other differentiate. The stem cell fate are tightly regulated by a combination of factors including cytokines, growth factors, transcription factors, chromatin modifiers and cell cycle regulators (Figure 1-7) (73). Hematopoietic stem cell (HSC) is the most common type of adult stem cells responsible for the regeneration of give rise to all the blood cell types. It has been used for treatment of leukemia for at least 40 years and recently been reported to be able to differentiate into a variety of specified cell types (74). For example, our lab proved that bone marrow derived cells are able to differentiate into retinal pigmented cells (51, 54). As a result, the stem cells are considered to be a potential source for the restoration of tissue function and a lot of clinical trials have been taken aiming to develop alternative treatment strategy for refractory disease(75). However, most of the stem cell treatments are passive in that there is no artificial regulation of the stem cell differentiation to certain direction. Understanding of the signal governing stem cell fate is extremely importance for the utilizing of stem cell as a medical treatment tool. There are mainly three signal transduction pathways that involve in the regulation of stem cell differentiation, the Wnt, Notch and Smad.

Wnt Signal Pathway

Wnt signaling plays an important role in the regulation of cell proliferation and stem cell differentiation (Figure 1-8). In the classic wnt pathway, β-caternin is the main actor. In the unstimulated situation, the free β-caternin is phosphorylated by the APC/Axin/GSK3β and degraded. When Wnt biding to its Fz receptor, APC/Axin/GSK3β complex is inhibited and β-caternin stabilized. Transcriptional activity of β-caternin/Tcf thus initiates the expression of series of genes.

Wnt signaling may regulate self-renewal of hematopoietic stem cells. Activation of wnt signaling pathway by soluble Wnt protein or over expression of β-caternin will promote proliferation and inhibit differentiation resulting in sustained self-renewal of HSC. Because of its function on stem cell proliferation and self-renewal, Wnt and their signaling mediators are attractive therapeutic agents (76). It is, however, paradox to find that the inhibition of Wnt signaling by sFRP2 will promote the restoration of the myocardial function by mesenchymal stem cell (70).

Notch Signaling Pathway

Notch signaling pathway plays pivotal role in the regulation of fundamental cellular process including stem cell maintenance and proliferation in adult and during development (Figure 1-8). After ligand binding, the intracellular part is cleaved off and enters the cell nucleus where it binding to RBP-J, to activates transcription of genes containing RBP-J binding sites. In the absent of ligand, the RBP-J works as a repressor for the Notch target gene through recruiting of corepressor. When the Notch signaling is activated, the released Notch intracellular domain will replace the co-repressor and result in the de-repression of genes containing RBP-J binding site. Consequently, the recruiting of co-activator will lead to the expression of Notch targeting genes.

Notch signaling pathway is a critical regulator in the stem cell maintenance. For example, Notch signaling inhibits neural differentiation through repressing the expression of proneural genes. Failure to activate Notch signaling will result in the formation of more neuronal clusters while constitutive activation of Notch signaling will suppresses neural differentiation in Drosophila. In vertebrates, Notch signaling is associated with stem cell maintenance. For example, activation of Notch signal will inhibit differentiation of crypt progenitors while post-natal gut specific inactivation of RBP-J results in the complete loss of proliferating transient amplifying cells in the gut (77).

Smad Signaling Pathway

The Smad signaling is implicated in the maintenance of pluripotency and self-renewal of stem cells (Figure 1-8). The signaling ligands include the TGF-β family proteins, bone morphogenetic proteins (BMPs) and activins. The signaling cascade begins when the ligands bind to the type II receptor which will recruit and activate by phosphorylate the type I receptor. Type I receptor is a single pass serine/threonine kinase receptors which can then phosphorylates receptor-regulated SMADs (R-SMADs). R-SMADs can bind the coSMAD and the R-SMAD/coSMAD complexes accumulate in the nucleus and regulate the transcription of target gene expression (78).

Smad signaling pathway plays important role in ESC self-renewal, maintenance of pluripotency and regulation of differentiation by exerting multiple and sometimes opposite effects depending on cellular context. It is currently believed the self-renewal promoting activity of animal serum is attributing to BMP2 and BMP4. It is believe the relative quiescence of HSC is due to the strong growth inhibition by TGF-β. However,

lower concentrations of BMP-4 induced proliferation and differentiation of primitive human hematopoietic progenitors. Because of its redundant function of Smad pathway which causes the embryonic lethality of knockout mice, the precise function on stem cells remains unclear. However, overall, the Smad signaling plays pivotal role in regulation of stem cell fate (73, 79).

PLK1 with Cancer and Cell Cycle

PLK1 is expressed primarily in proliferating cells due to its crucial role in numerous mitotic events (Figure 1-9) (80). Overexpression of PLK1 is an early event of cancer cells and inhibition of PLK1 activity results in a potent antitumor effects both in vitro and in vivo suggesting that PLK1 can be act as oncology targets (81). A recent study on zebrafish heart regeneration suggests that PLK1 is an essential component of regeneration (82). Upon the observation that p21 and PLK1 are involved in regeneration and the fact that both play critical role in cell cycle regression, we hypothesized that cell cycle regulation genes are essential for regeneration and the modification of the expression level to mimic that of wound healing mice strains may reproduce the regeneration in normal mice.

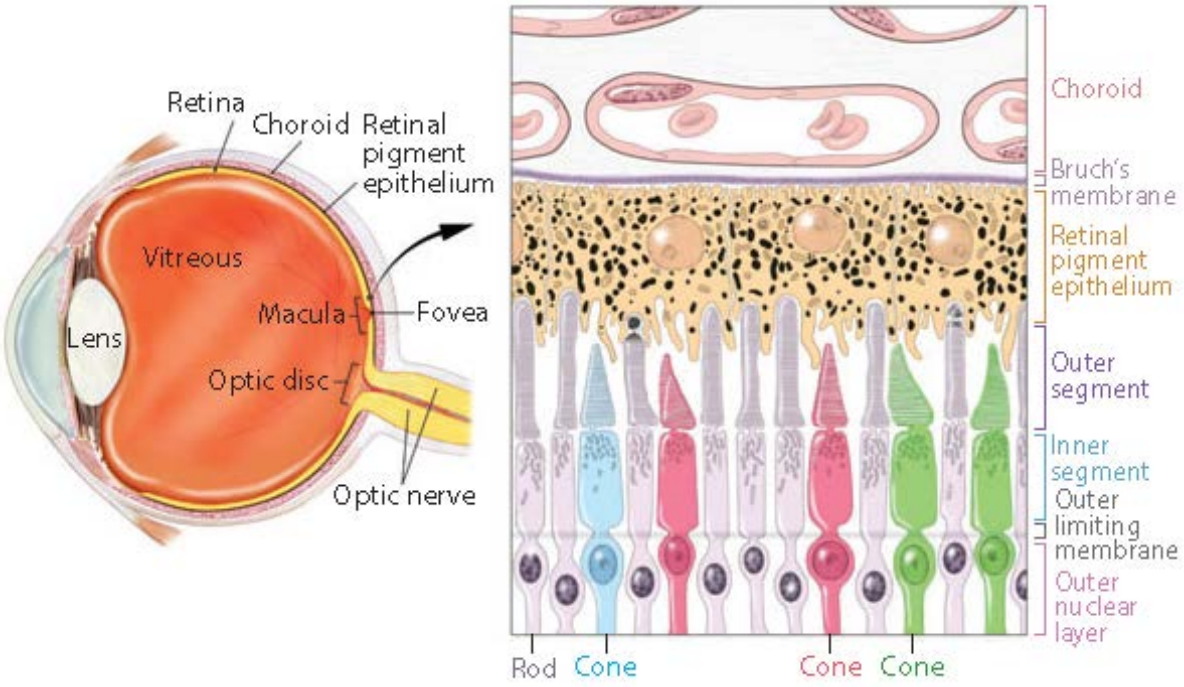

Figure 1-1. Schematic diagram of healthy retina and illustration of layers of the neural retina. Cone cells are in red, green or blue (8).

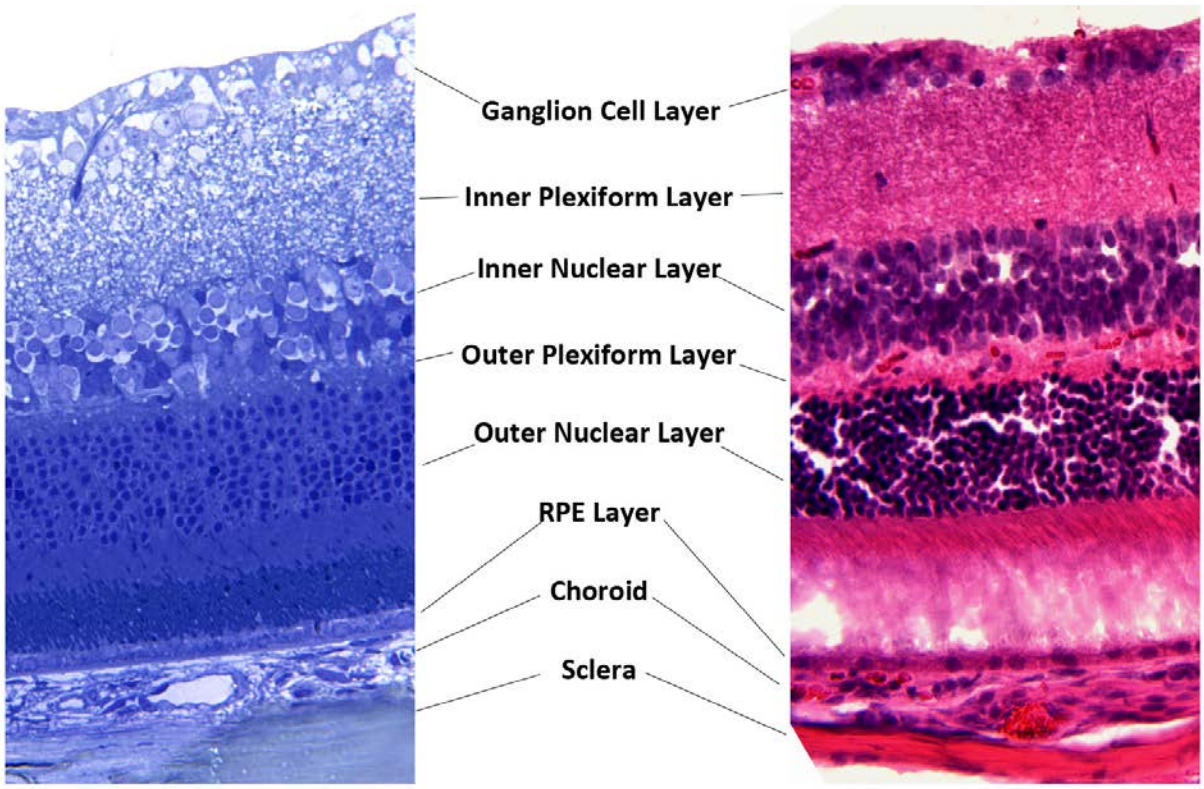

Figure 1-2. Layers of neural retina illustrated by H.E. staining of cryosection of posterior cup and plastic embedding sectioning stained with toluidene blue.

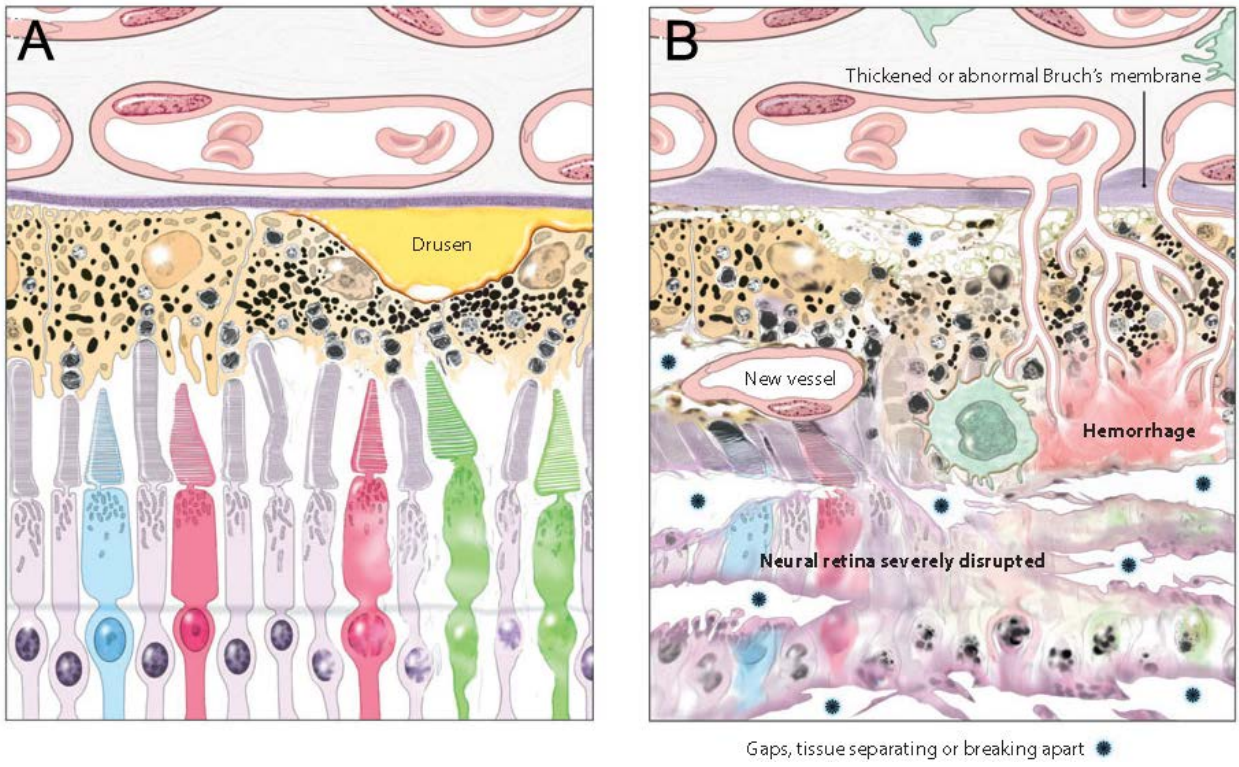

Figure 1-3. Retina structure under age related macular degeneration. A) Diagram of the posterior cup subretinal region with early sign of AMD. B) Diagram of the posterior cup subretinal region with wet-AMD (8).

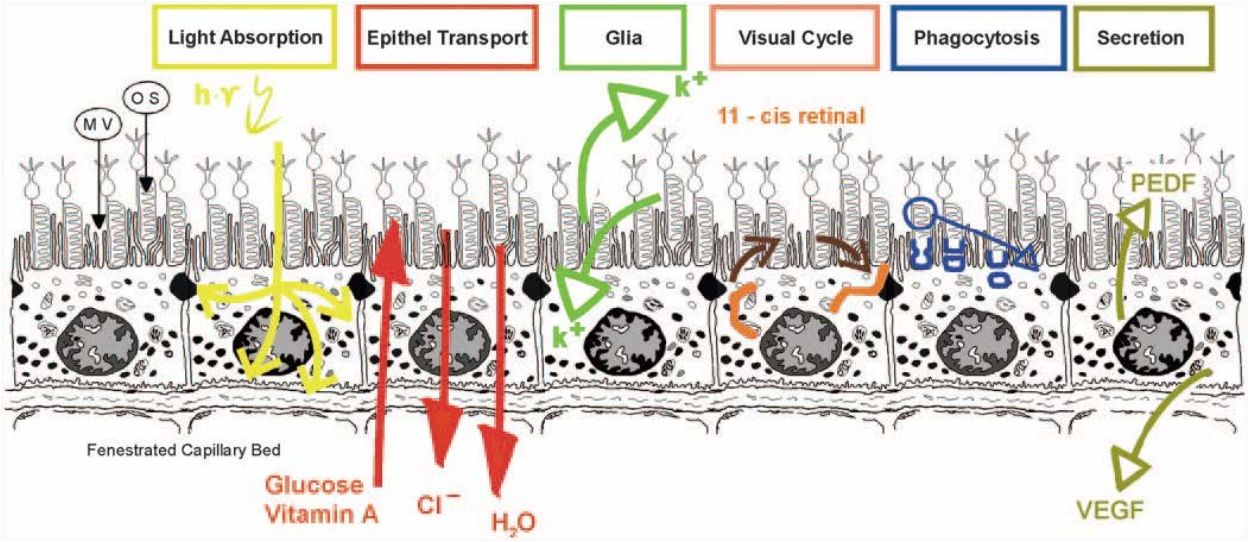

Figure 1-4. RPE cell layer as an indispensable part for vision function (12).

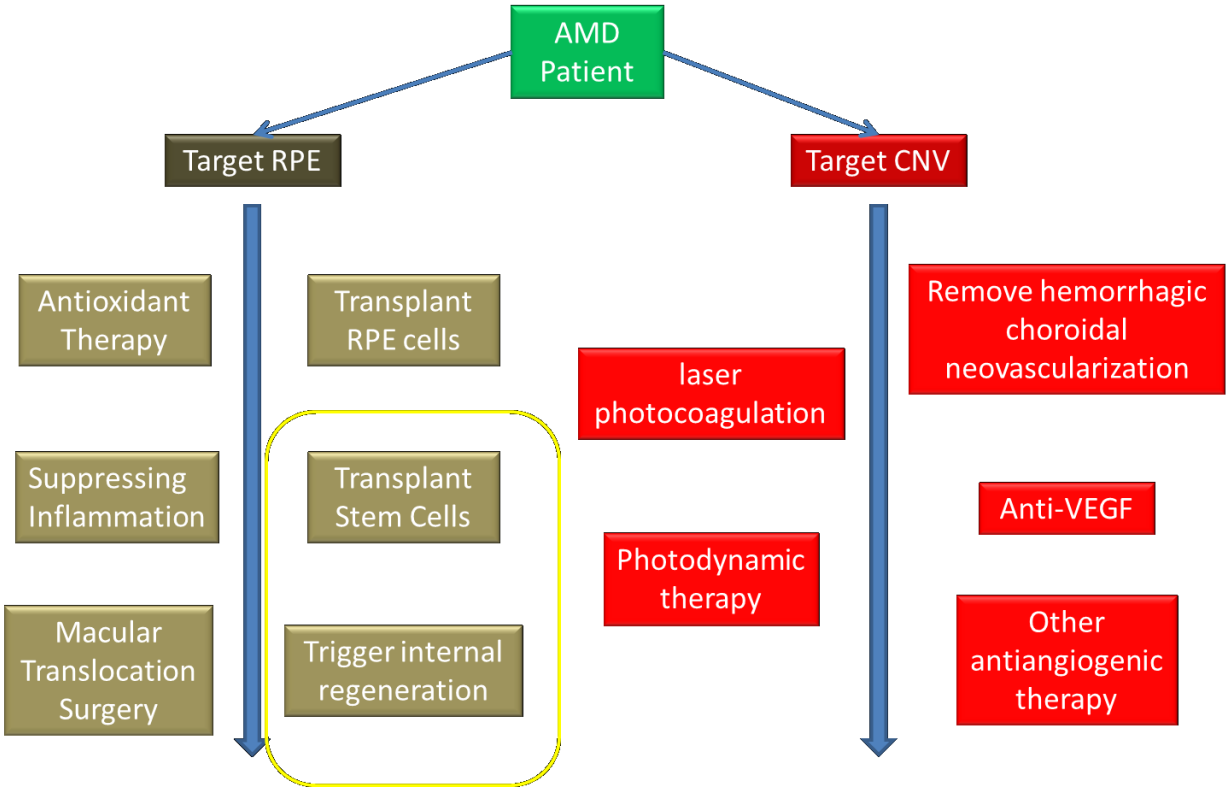

Figure 1-5. Strategies of AMD treatment.

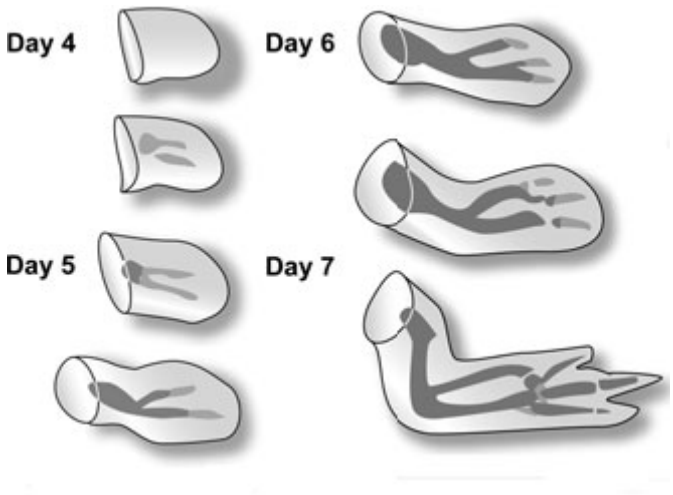

Figure 1-6. Illustration of limb regeneration (59).

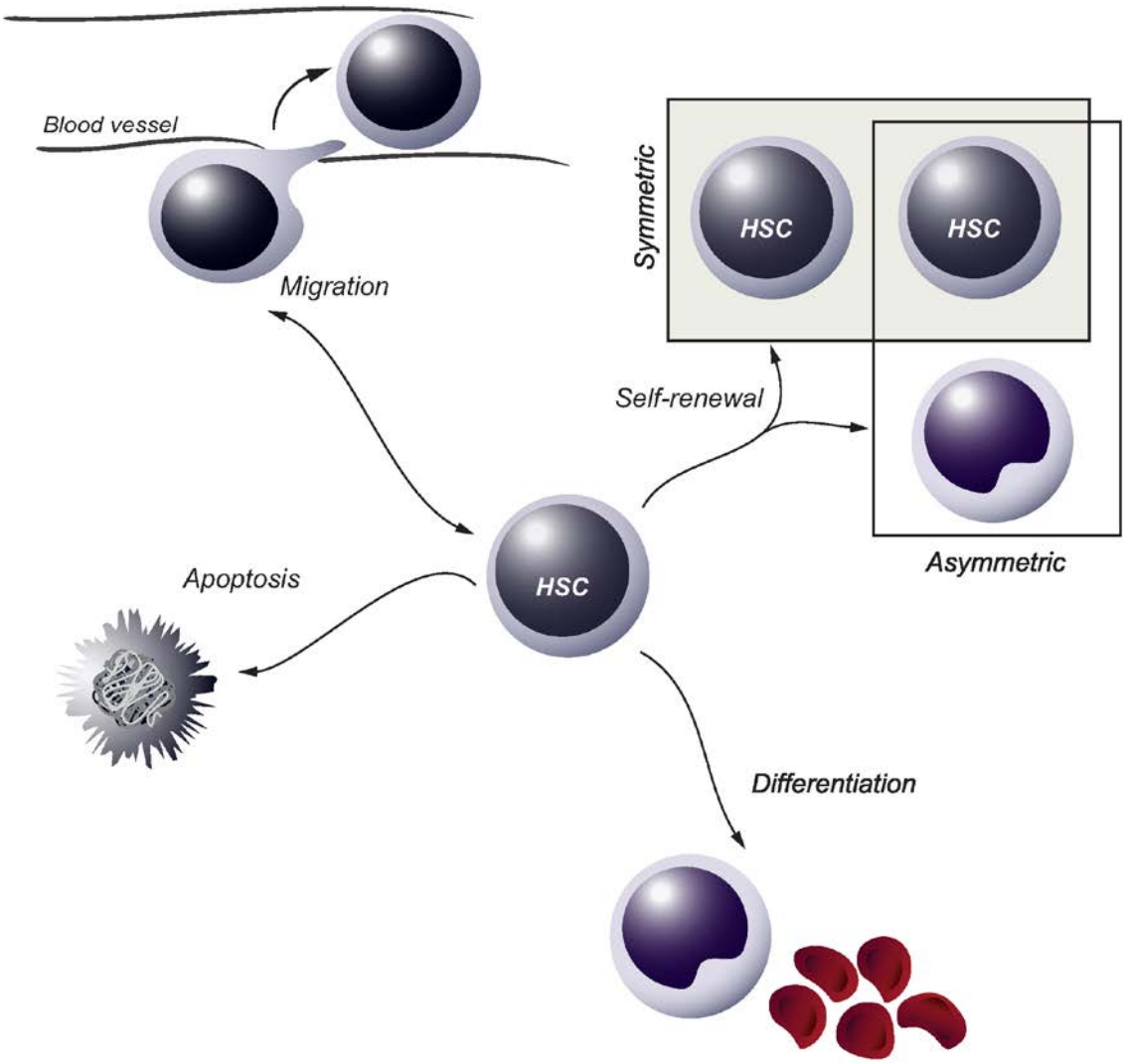

Figure 1-7. HSC fate decision (73)

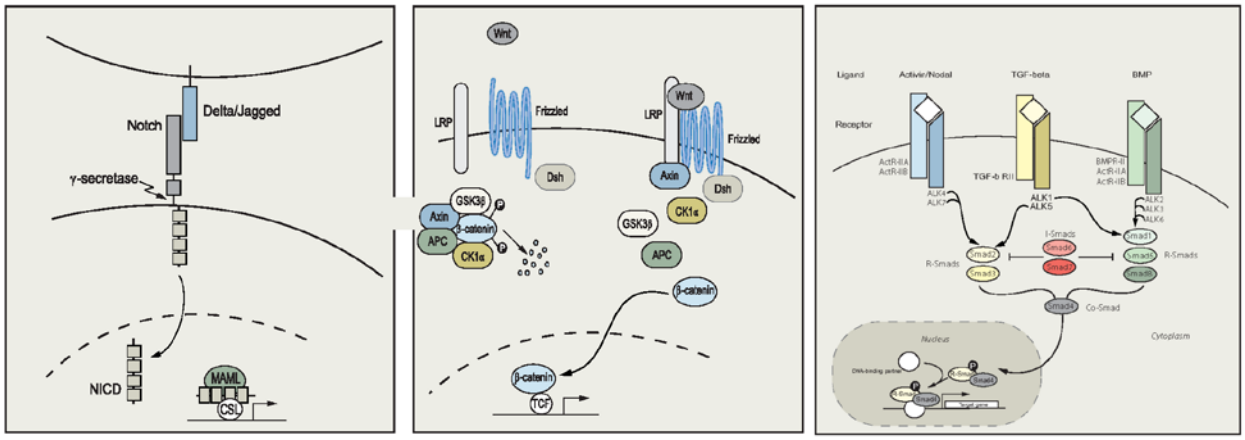

Figure 1-8. Notch, Wnt and Smad signaling pathways (73)

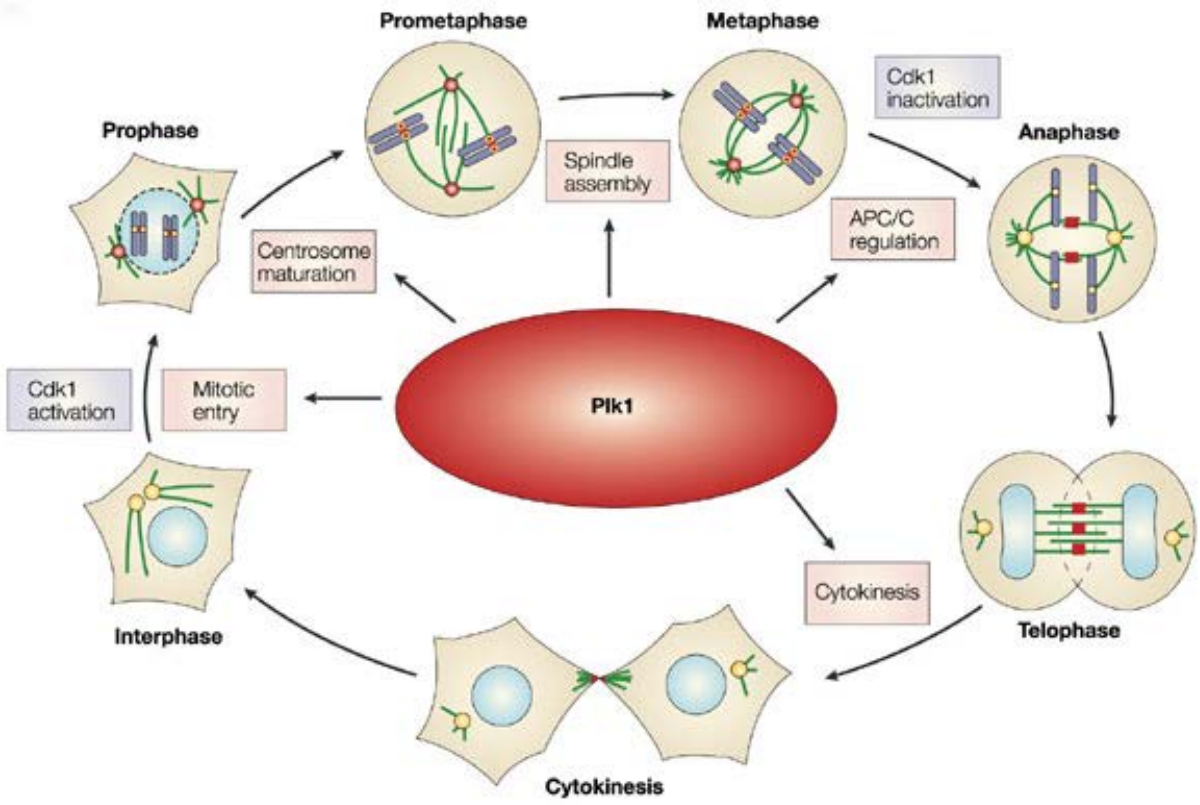

Figure 1-9. PLK1 and cell cycle regression (80)

CHAPTER 2
MATERIALS AND METHODS

In this chapter, the main method utilized for accomplishing this thesis is described. The materials and methods described in this section are optimized over a number of years from multiple previous reports and own observations. All animal procedures were reviewed and approved by the University of Florida Animal Care and Use Committee and performed in an Association for Assessment of Laboratory Animal Care approved facility according to the regulations in the ARVO Statement for the Use of Animals in Ophthalmic and Vision Research. A general flowchart of the experiment is given in Figure 2-1. The details of each procedure are described in following sections.

Animals

MRL/MpJ and B6.129S6(Cg)-Cdkn1atm1Led/J mice were obtained commercially (Jackson Laboratory, Bar Harbor, ME). Two ancestral strains of MRL/MpJ, AKR/J (Jackson Laboratory) and C57BL/6 (Charles River Laboratories, Wilmington, MA) were chosen as albino and pigmented control strains, respectively. For studies of pigmented animals, MRLBL/GFP, a laboratory derivative of MRL/MpJ mice was used. This strain was constructed by crossing MRL/MpJ and Tg (CAG-EGFP)B5Nagy/J mice (Jackson Laboratory) to obtain black mice expressing green fluorescent protein (GFP), which were then backcrossed against MRL/MpJ for >5 generations with retention of these phenotypes. Ear punch closure analysis confirmed the regeneration phenotype. Mice were raised on cage racks with unrestricted access to food and water under fluorescent lighting with a 12-hour light/12-hour dark cycle.

Sodium Iodate Administration

Sterile sodium iodate (Sigma-Aldrich, St. Louis, MO) in 1xDulbecco's phosphate buffered saline (PBS, Gibco. Carlsbad, California, 14190136) at dose of 20-40mg/kg was injected into adult mice (weighting ~35 grams for MRL/MpJ and MRLBL/GFP, ~20 grams for other strains) through retro-orbital sinus. The sodium iodate stock solution was prepared by dissolving 20 mg of sodium iodate into 2mL of sterile 1xPBS. The stock solution was then filtered through 0.22 µm syringe filter (Fisher Scientific). This led to a sterile solution at concentration of 10mg/ml. Further serial dilution by adding appropriate volume of sterile 1xPBS yielded the solutions at the concentration of 7.5 mg/ml and 5 mg/ml. All the mice were weighted and injected proportionally with x µl of sodium iodate solution where x=body weight (in gram)*4. For mice treated with 20mg/kg, 30mg/kg and 40mg/kg dose were injected with the 5 mg/ml, 7.5 mg/ml and 10 mg/ml solutions respectively. Untreated animals were injected with a comparable volume of PBS. RPE injury was monitored at 5 days, 30 days and 60 days period by RPE/sclera flatmounts and retinal cross-sections (refer to corresponding sections for more details). For the sodium iodate treatment of mice with whole bone marrow transplantation, sodium iodate was injected 4 days ahead of the irradiation.

Irradiation and Bone Marrow Transplantation

Bone Marrow Cell Collection

Adult donor mice were euthanized and the long bones in the legs (femurs and tibias) were immediately excised. All muscle, tendon, and ligature were peeled to the end of joint by hand and cut by the blade discarded. The long bones were immediately immersed in ice-cold 1x PBS supplemented with 2% Fetal Bovine Serum (FBS; Gibco) and was cut on each end to expose the marrow cavity trabecular region. The bone

marrow was was flushed out into a tissue culture treated plate by inserting a 26 ½ - gauge needle into one end of the bone and washing ~3 mL of PBS with 2% FBS through the hollow bone core by quickly push the cartridge of 3ml syringe. By pipetting using a 1 ml pipette and through a 18-gauge needle, the bone marrow was manipulated into single cell suspension. The cell suspension was then filtered through the BD Round-Bottom tube with cell strainer cap to get rid of debris (BD 352235). The filtered cell suspension was then pelleted by centrifugation at 1000 x gravity performed at 4° Celsius (°C). The pellet was then counted and resuspended in 1x PBS with 2% FBS with appropriate volume. More than 10^5 donor cells were injected to each recipient mouse.

Irradiation and Bone Marrow Cell Injection

The mice received 950 Rads of whole body irradiation. The bone marrow transplantation was conducted by retro-orbital injection (83). Before injection, the mice were anaesthetized briefly with isofluorane (Baxter; Deerfield, Illinois). The anesthetized mice was positioned on its side and restrained with thumb and middle finger of non-dominant hand. By gently pressing the surrounding tissue, the eyeball was pushed out and needle was inserted at approximately 45 degree beneath the globe of the eye, piercing through the conjunctiva and directly into the retro-orbital sinus. No resistance, the feeling of bump up by the non-dominant finger, and a little bit blooding is a sign of correct injection. A sharp cutting needle is preferred in order to minimize tissue distortion and damage. The volume of injection is up to 200 µl. The bone marrow cell suspension (~10^5) was administrated as described. The irradiated and bone marrow transplanted mice was then watered with 2.5 mL antibiotics supplement Baytril 100 (100

mg/ml, enrofloxacin,Bayer HealthCare; Shawnee Mission, Kansas) into 500 mL water bottle, for minimum of two weeks.

Electroretinography (ERG)

Mice were dark-adapted overnight before analysis. Pupils were dilated with 0.5% proparacaine hydrochloride (Akorn, IL) and 0.5% phenylephrine hydrochloride (Bausch and Lomb, FL). Mice were anesthetized with avertin at 0.5 mg/g body weight. The mice should be anesthetized completely (otherwise will generate noise) and placed on a temperature-controlled working platform at 37°C. Gold-rimmed contact electrodes were placed on the corneal surface and visual responses were recorded with a UBA 4204 visual electrodiagnostic ERG system (LKC Technologies, Gaithersburg, MD) using white light stimuli at intensities of -45, -35, -25, -15, -5 and 5 dB with LED light. After the measurement, the mice eyes were applied with vetropolycin and put on the 37 °C slide warmer. The ERG traces were recorded and exported as CSV files which were used for analysis by using Office Excel software.

Mouse Eye Preparation

Cardiac Perfusion

To get better morphology of the eye in histological analysis, the mice were fixed by myocardial perfusion with 4% paraformaldehyde (PFA). Prior to perfusion operation, the mice were anesthetized with an intraperitoneal (I.P.) injection of 240mg/kg avertin (2,2,2-Tribromoethanol, Sigma-Aldrich). Deep anesthetized mice were spread-eagle on a dissecting board with 20-gauge needles. The lower limbs were spread very far apart whereas the upper limbs should be secured closer to the body of the animal to relieve tension on the thorax. 70% alcohol was spread on the mice body. Made a shallow cut on the fur of the mice abdomen by using forceps and a scissor. The fur on the abdomen

was torn apart along the cut in the vertical direction to spinal. Made a cut on the upper part of the fur and using hand to tear the furs along the midline of the body. The abdomen was then opened without cutting on the visceral or blood vessels. Thoracic cavity was then opened up by making side cuts and with an 18-guage needle to fix the surrounding tissue to the board. In the hood, by using a switch valve, which has one side installed 3ml syringe of 1x PBS and the other side with 5ml syringe of 4% PFA, perfuse the mice first with PBS and then with 4% PFA. The perfusion was operated as follows: slowly insert the 26 ½ -gauge needle into the left ventricle, and made a punch on right atrium with another 26 ½ -gauge needle, slowly pressed the cartilage to perfuse the 1x PBS through the circulating system. After “washing” the system with 1xPBS, switched the valve and continue the perfusion with 4% PFA. With successful perfusion, we could see the leaking of blood from the right atrium and turning from red to whit of the lungs as well as hardening of the body.

Mouse Eye Analysis

The perfused mice from last step was blew with air for 30 second to make the eye dry and marked at the 12 o'clock point of the eye to make the orientation of the eye in following steps easier. Eyes were carefully enucleated by digging into the eye with sharp blade and with gentle to to preserve the morphology as much as possible. In 1x PBS, extraocular tissue were carefully removed the by using bonn forceps (World precision instruments, 555055FT). The processed eye balls were put the in 4% PFA for 5 minutes and removed the anterior part (cornea and lens) of the eye by using bonn forceps and westcott stitch scissors (Katena products, K4-4100). Cutting around lens to disconnect the lens from iris will make the enuleation of lens easier. Made a minor single cut on the marked 12 o'clock point. With one of the posterior cup, made 5-6

radical cuts extending to optic nerve to flatmount the eye. Depending on different purpose, either separate the retina from the RPE-chroid-sclera or leave it as a whole mount (84). The second eye was transferred it to a 24 well plate well with 4% PFA and fix for overnight. After fixation the eye cup was transferred to 20% sucrose in PBS for overnight at 4°C and to 30% sucrose in PBS for another overnight incubation at 4°C and finally to 30% sucrose supplemented with 20% tissue freezing medium OCT (Optimal Cutting Temperature compound, VWR 25608-930) and incubated overnight at 4°C. By using forceps, the eye cups were slowly put into the cryomold (Tissue-Tek, Biopsy, 62534-10) with OCT and oriented under dissecting microscope carefully to prevent bubbles. 2-methyl butane (Fisher 03551-4) was poured into a container with dry ice. The tissue (in cassette and OCT) was then slowly placed in dry ice/2-methylbutane mixture making sure that the exposed OCT never touches the liquid until it is frozen solid to prevent bubbling of OCT. When the tissue in OCT was frozen, the block was marked and placed in -80°C freezer.

Flatmount Staining and RPE imaging

OCT Sectioning

The OCT blocks were transported on dry ice to sectioning machine and let it sit for 5 minutes for equilibrate to cryostat temperature (~-20 °C). After marking the 12 point, the block was attached to the holding knob of the sectioning machine with OCT for at least 5 min. Blocks were oriented and serial cut at 14 µm thickness and sections collected onto the positive charged slides (Superfrost/Plus, Fisher Scientific, Pittsburgh, PA). Every four sections were collected per slides. All the slides were dried under room temperature overnight and placed in -80°C freezer. Sections with optic nerve were selected for further imaging.

Immunohistochemistry

For immunohistochemistry, sections were treated with target retrieval solution (DAKO, Carpinteria, CA), protein blocking buffer (DAKO), and biotin and avidin blocking kit (Vector Laboratories, Burlingame, CA). Sections were stained with mice anti-RPE65 antibody (401.8B11.3D9, NOVUS, Littleton, CO) at 1:150 dilution as primary and donkey anti-mouse IgG AlexaFluor 488 (Invitrogen, Carlsbad, CA) at 1:500 dilution as secondary by using ARK kit (DAKO). After extensive washes in Tris-buffered saline, the slides were counterstained and mounted in antifade medium (Vectashield; Vector Laboratories) with 4'-6-diamidino-2-phenylindole (DAPI). Microscopy was performed with a spinning disk confocal microscope (BX61WI-DSU; Olympus, Center Valley, PA). Green and blue channels were acquired with a 20X objective and merged with Volocity (Perkin Elmer) and tiled with the MosaicJ plugin (85) in ImageJ (Wayne S. Rasband, U. S. National Institutes of Health, Bethesda, Maryland, USA; available at http://rsb.info.nih.gov/ij/download.html)

Plastic Sectioning

To check for morphological changes after injury, harvested eyes were fixed overnight in 2% glutaraldehyde and 4% paraformaldehyde in PBS. The eye cups were washed in Cacodylate (pH 7.4) for 3x10 minutes and then transferred to 1% osmium for 4 hours at 4°C and embedded in epoxy resin. Sections were cut at 1 µm thickness and stained with toluidine blue (86).

Flatmount

For whole mounts, left posterior eyecups were stained at room temperature with DAPI and rhodamine-phalloidin (Invitrogen, Carlsbad, CA) in PBS containing 1% Triton X-100 for ≥24 hours. Eyecups were cut radially, mounted with Vectashield and imaged

with a spinning disk confocal microscope (IX81-DSU or BX61WI-DSU; Olympus, Center Valley, PA) with acquisition software (Slidebook, Olympus; or Volocity, respectively).

Brdu Staining for Proliferation

Bromodeoxyuridine (BrdU, Sigma-Aldrich, St. Louis, MO) incorporation was used to observe cell proliferation after injury. Prior to Brdu injection, the mice (MRL/MpJ and AKR/J mice), were treated with sodium iodate at the dose of 20mg/kg body weight. The 100 mg Brdu powder was dissolved in 10ml 1x PBS to make it a 10mg/ml solution. The sodium iodate treated mice were administered daily with 5 fold body weight (g) volume (µl) of the Brdu solution by intraperitoneal injection to the dose of 50 mg/kg body weight. Eyes were harvested 30 days post sodium iodate injection. Eye cups were embedded in OCT. The OCT blocks were sectioned, antigen retrieved with 0.1% Trypsin for 7 minutes at 37 °C, and stained with the BrdU staining Kit (Invitrogen, Carlsbad, CA, 93-3943). Pictures were taken under bright field. By creating and subtracting a blank background will improve the quality of the image.

Microinjections

There are various administration options for the delivery of therapeutic reagents to the eye. Figure 2-2 gives an illustration of mice eye and the injection delivery sites. Injection of compound precisely and with minimum of trauma is desired to maximize treatment effect.

Intra-Vitreal Injection

Intravitreal administration of drugs is a popular method used to treat many retinal diseases, including AMD. Prior injection, sterile injection reagents should be prepared and placed on ice. Hamilton 901 N 10 µL Syringe was washed first with water and later with 70% alcohol and dry in the hood. After anesthetize animals with avertin, the

treatment reagents (stem cells, drugs et al.) was drawn into tuberculin syringe from a sterile bottle with thirty two gauge needles (blunt). Gonak (Akorn, IL) was applied to prevent hemorrhage during the injection. At the site of the infero-temporal quadrant, a shallow punch was made with the Insulin syringe 28G1/2. The blunt needle of Hamilton 901 N 10uL Syringe was slowly inserted through the punch into the intravitreal space. The cartilage of the syringe is pushed by assistant slowly to avoid jet formation or cavitary flow. Using a single smooth continuous maneuver, the treatment agent was injected into the eye. Gently and slowly remove the needle from the eye. Multiantimicrobial drug was applied to avoid infection and placed on the slide warmer for better recovery. Sometimes the fluorescein isothiocyanate (FITC, Sigma-Aldrich, St. Louis, MO) was used as an indicator to track the treatment drug. A successful injection will lighten up the eye with minor fluorescein flow out. The maximum volume of intra-vitreal injection is up to 2 μl for adult mice (59).

Subretinal Injection

The subretinal space is an excellent target site for RPE loss treatment. It is commonly used clinically and has been used in many animal models including mice. Like intravitreal injection, sterile injection reagents should be prepared and placed on ice. Hamilton 901 N 10uL Syringe was washed first with water and later with 70% alcohol and dry in the hood before injection. Prior anesthetizing, the mice pupil was dilated with first with atrophine sulfate (Bausch&Lomb) twice every half hour and then phenylephrine (Bausch&Lomb) once. Under deep anesthetization, the mouse was positioned with its nose pointing away from the surgeon. A drop of gonak was applied to prevent hemorrhage. By gently tightening the surrounding tissue, the eye was pushed

little bit out. A sharp 26 ½ -gauge needle was used as a lance to make a punch on the cornea. The thirty two gauge blunt needle was advanced to the retina opposite to the puncture site until it was but a few tip diameters away from the optic nerve head. The view of needle tip was magnified by the lens. By a gentle pressure was applied to penetrate the neural retina into the subretinal space. Too much pressure will penetrate or damaged the RPE sheet. Appropriate extent of press can only be judged according the experience and feeling. By slowly press the cartilage of the syringe, the treatment agent was slowly delivered to the subretinal space. Slowly pull out the needle and apply vetropolycin (Nada # 065-016). The maximum injection volume of subretinal injection is up to 2 µl (73).

Fluorescence-Activated Cell Sorting (FACS)

Peripheral blood was collected through the saphenous vein of the cheek using a 5.0 mm GoldenRod animal lancet (MEDIpoint, Inc. Mineola, New York) by dropping 5-8 blood drops into a 5mL falcon tube (Fisher Scientific) containing 0.5 mL of 1X PBS and 5 mM EDTA which act as an anticoagulant. Peripheral blood mononuclear cells (PBMC) were collected apart from the erythrocytes and granulocytes by using Ficoll-Paque™ PLUS (Amersham Biosciences. Uppsala, Sweden) purification. 1.5mL of Ficoll-Paque™ PLUS was conducted to the bottom of the blood/PBS mixture by using a Pasteur pipette. This solution was centrifuged at 1000rpm at 4 °C for 40 minutes. PBMC will be located in the cloudy layer of the stratified blood sample. By using Pasteur pipette, the PBMC were collected into new 5mL falcon tubes where the cells were washed in 5x volumes of 1x PBS and then blocked in 10% normal rat serum for 30 minutes at 4°C. Antibodies (0.5 µg/µl (1 µl) of antibodies to CD3e (T cells), CD11b (macrophages), B220 (B cells), CD117, Scar1 and IgG control antibodies (for exclude

non-specific binding) conjugated to FITC (BD Pharmingen) were used to label collected PBMC cell. After staining, the cells suspensions were washed in 5x volumes of 1x PBS and resuspend in the left-over solution. FACS was performed by using FACScaliber (BD Biosciences).

Realtime Reverse transcription PCR

Mice tissue was collected and put in RNAlater (Qiagen, 76104) and homogenized with the molar. RNeasy mini kit (Qiagen, 74104) was used to extract RNA. cDNA was synthesized by using SuperScriptTM III First-Strand Synthesis System (Invitrogen, 18080-051). Realtime PCR primers are obtained from the following website:

http://pga.mgh.harvard.edu/primerbank/

http://mouseprimerdepot.nci.nih.gov/

QuantiTect SYBR Green PCR Kit (Qiagen, 204141) was used to compare the mRNA expression level of different genes. Beta-actin mRNA expression level was used as an internal standard. Each sample was triplicated in the assay carrying out in the 96 well plate.

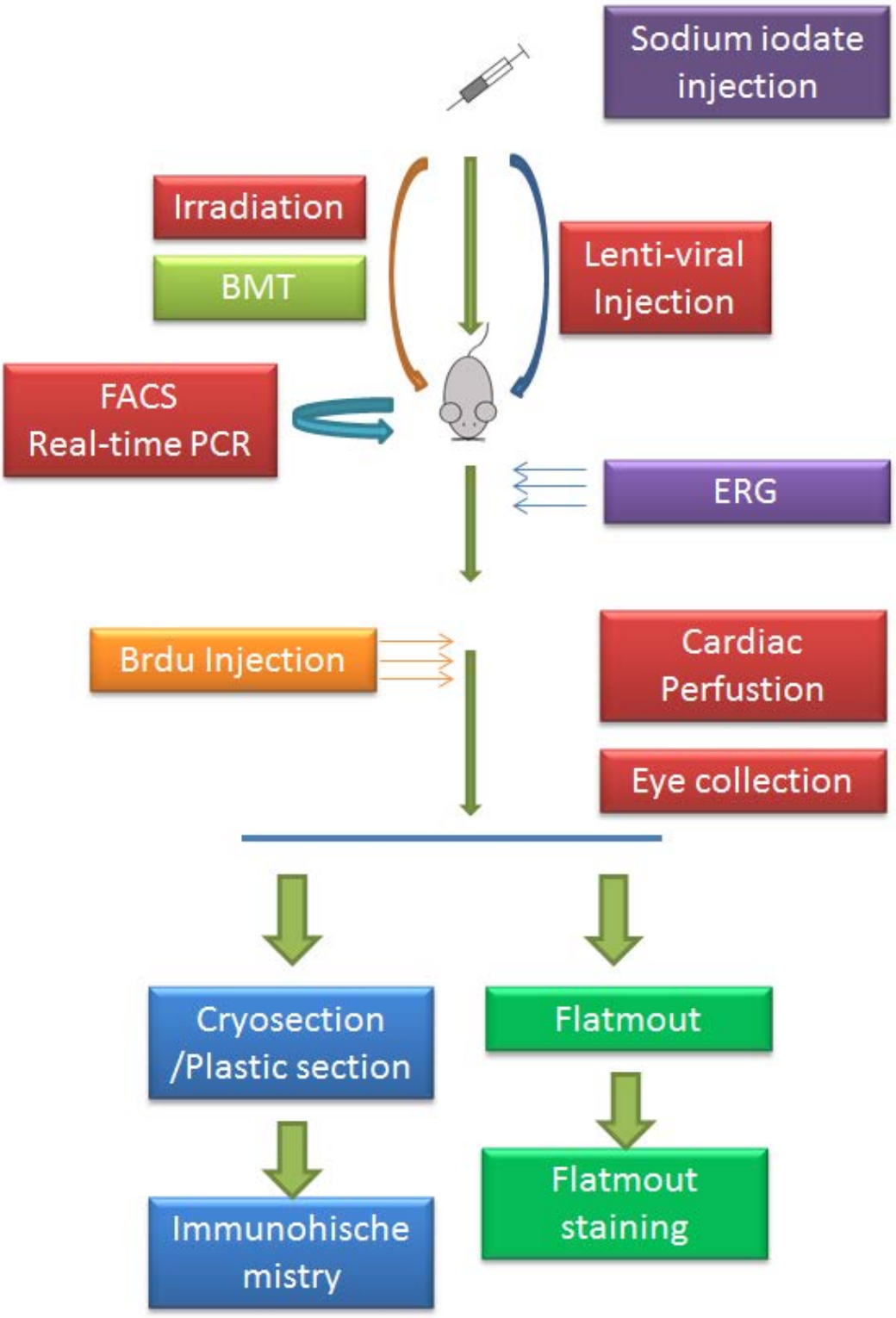

Figure 2-1. Overview of the experiment design.

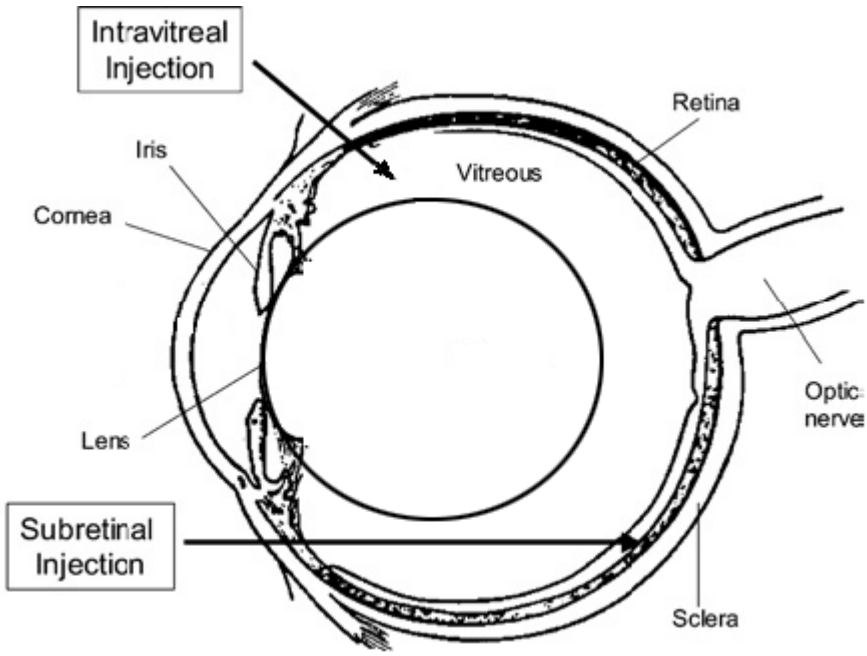

Figure 2-2. Schematic diagram showing different routes of ocular delivery, including intravitreal and subretinaled after cell division (87).

CHAPTER 3
SODIUM IODATE DAMAGE TO RPE AND OPTIMIZING DOSAGE FOR REGENERATION

Sodium iodate has been used for several decades as a specific toxin of RPE. Though the complete mechanism is not well understood, sodium iodate has been shown to inhibit lysosomal enzyme activities within RPE cells, especially acid phosphatase activity, which is essential for RPE cell survival and normal function (88). The area and the extent of damage is sodium iodate dose dependent. Low dose (15, 20mg/kg) of sodium iodate cause specific damage on RPE and around the central retina, while high dose of sodium iodate cause a more dramatic damage affecting a vaster area including the peripheral region and damage not only RPE but also photoreceptor cells (60, 61). To develop a model for RPE regeneration, we sought to induce damage and compare functional and morphological recovery of the RPE in MRL/MpJ with other strains. An immediate issue was the choice of control strains. MRL/MpJ is an inbred albino strain initially generated from a series of crosses among several laboratory strains, making congenic comparison impossible. Albino strains have also been reported to be more sensitive to sodium iodate induced RPE damage (89). We chose control strains with normal wound-healing capability, including C57BL/6 and AKR/J, which were used as stock in the generation of MRL/MpJ mice. Furthermore, AKR/J serves as an albino control for the pigmented C57BL/6 strain. We also have crossed the MRL healer phenotype onto a pigmented GFP-positive background to generate MRLBL-GFP as a pigmented counterpart of albino MRL/MpJ for our study.

Validation of Regeneration Phenotype by Ear Punch

To begin with, we have to validate that the strains we were using does have the regeneration ability, especially MRLBL-GFP for the reason that it has been cross

breeded with non-regeneration strain. Ear punch was adopted since it is simple, straightforward and visible. Adult C57BL/6, MRL/MpJ and MRLBL-GFP at the age of approximately 4-5 weeks old were through-and-through ear punched, the closure of the ear punch was photographed at week 1, 2, 3 and 5 (Figure 3-1). We found that the ear hole was recovery and almost closed on the third week after the punch both on MRL/MpJ and MRLBL-GFP but not in C57BL/6 indicating that MRL/MpJ and MRLBL-GFP have enhanced wound healing ability.

Comparison the Regeneration Under 40 mg/kg Dose

To avoid possible secondary effects that might hinder regeneration (51), our first objective was to identify conditions in which recovery of injured RPE in MRL/MpJ mice could be easily distinguished from that of control mice. In many mouse studies of RPE injury (51, 54), sodium iodate was used at a dose of 40 mg/kg body weight or higher. This dose resulted in substantial RPE damage with minimal recovery in preliminary experiments. In our initial trials, we used the 40mg/kg body weight to compare the regeneration between the C57BL/6 and MRL/MpJ, the wound healing strain. The regeneration was observed to be more robust in MRL/MpJ than in C57BL/6 by ERG analysis, by morphology and by the outer nuclear (ONL) thickness measurement (Figure 3-2, Figure 3-3). Moreover, intra-vitreal injection of CD133+ cells were conducted at the dosage of 40mg/kg with the same protocol as described previously (54).Though donor derived cells were observed to differentiate into RPE-like cells (Figure 3-5), the occurrence and efficiency is not stable. In all, the regeneration under 40 mg/kg sodium iodate treatment was not stable and robust as we expected, possibly due to the reason that the regeneration environment was destroyed at 40 mg/kg dose.

The regeneration observed in MRL/MpJ mice under this dose was far from being significant for future investigation and for clinical trials.

Optimizing Sodium Iodate Dose

We hypothesized that high-dose sodium iodate may cause excessive damage to the tissue microenvironment, leading to the loss or alteration of repair signals and environmental guidance cues that are required for regeneration. Massive damage would most likely lead to scar formation regardless of strain background. Four mice strains (C57BL/6 vs MRLBL/GFP, AKR/J vs MRL/MpJ) were injected retro-orbitally with sodium iodate at various doses (20, 30 and 40 mg/kg body weight) and examined one month later by ERG. One month is a time point when a plateau stage has been reached in C57BL/6 mice injected with low dose of sodium iodate (60). Significantly greater b-wave amplitudes were observed in MRL/MpJ and MRLBL/GFP mice compared with all other strains tested at all sodium iodate doses. The differences in ERG amplitudes between MRL/MpJ, MRLBL/GFP and control cohorts were greatest at a dose of 20 mg/kg body weight. The 20 mg/kg dose also resulted in a near flat line ERG response in the control strain that was not significantly different from the damage observed with higher doses of sodium iodate. Moreover, regardless of pigment phenotype, MRL strains showed a more robust recovery of the ERG signal than control strains (Figure 3-4), suggesting that the previously reported influence of pigment on sodium iodate susceptibility (89) does not apply to recovery. In all, sodium iodate will cause selective toxic effect on RPE cell layer. MRL/MpJ mice were able to recover from sodium iodate damage at low rate. High dose of sodium iodate can cause detrimental effect on regeneration. 20 mg/kg is a dose where the recovery difference can be amplified. Based on these results, we chose a sodium iodate dose of 20 mg/kg for further studies.

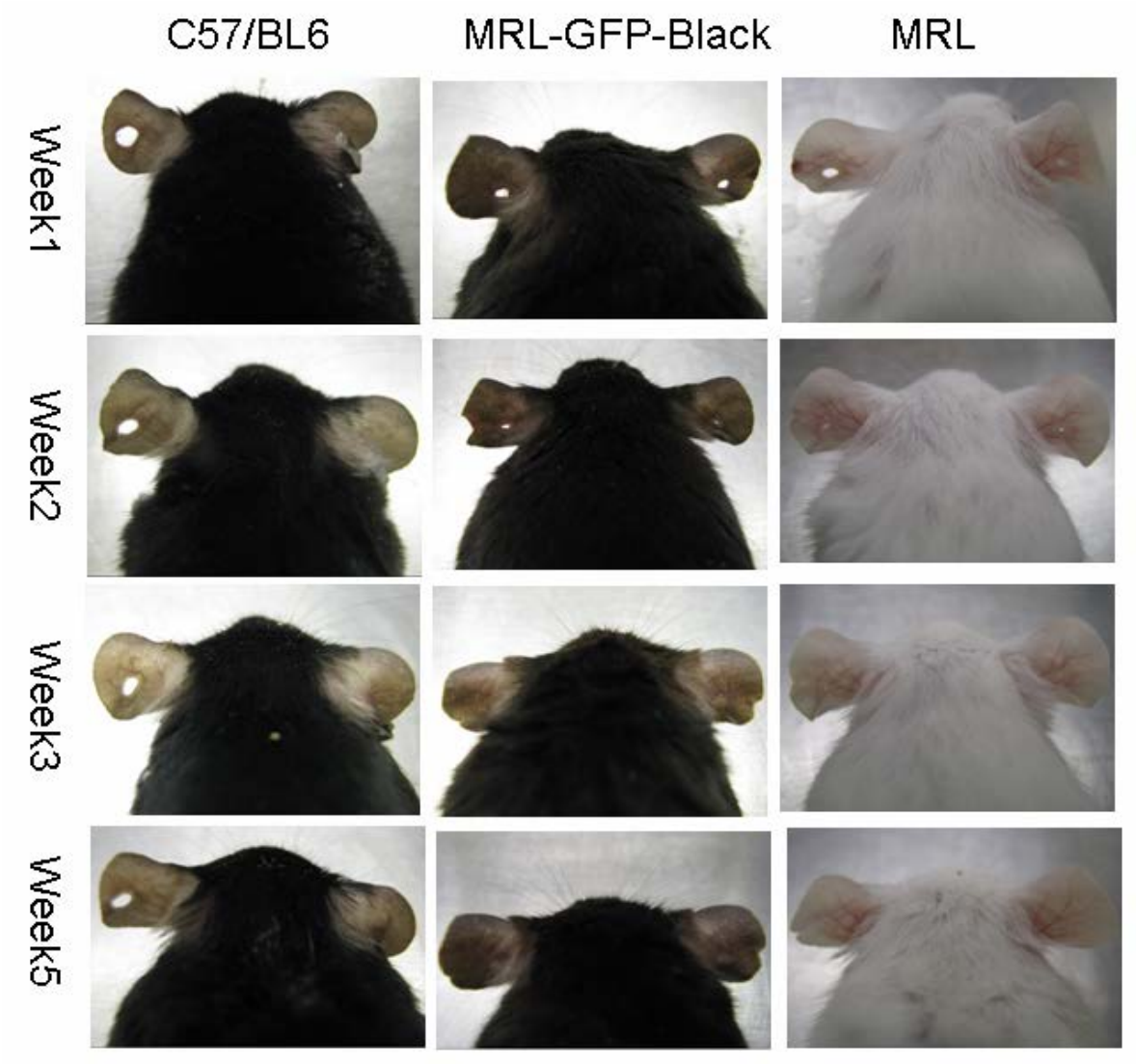

Figure 3-1. Confirmation of the MRL-GFP-Black wound healing phenotype. Bothe MRL/MpJ and MRL-GFP-Black mice were able to completely close the ear punch.

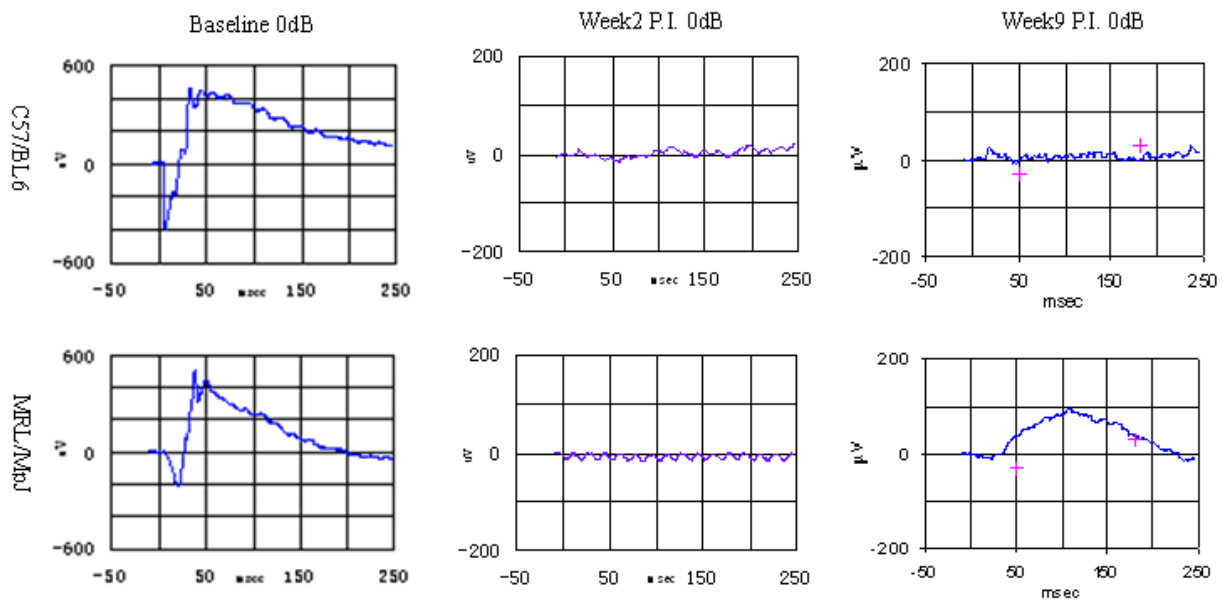

Figure 3-2. Comparison of ERG signaling between C57/BL6 and MRL/MpJ after 40mg/kg of sodium iodate (Note: y axis change) There is difference on the response to the sodium iodate injury. MRL/MpJ strain was able to recovery at low rate after sodium iodate damage.

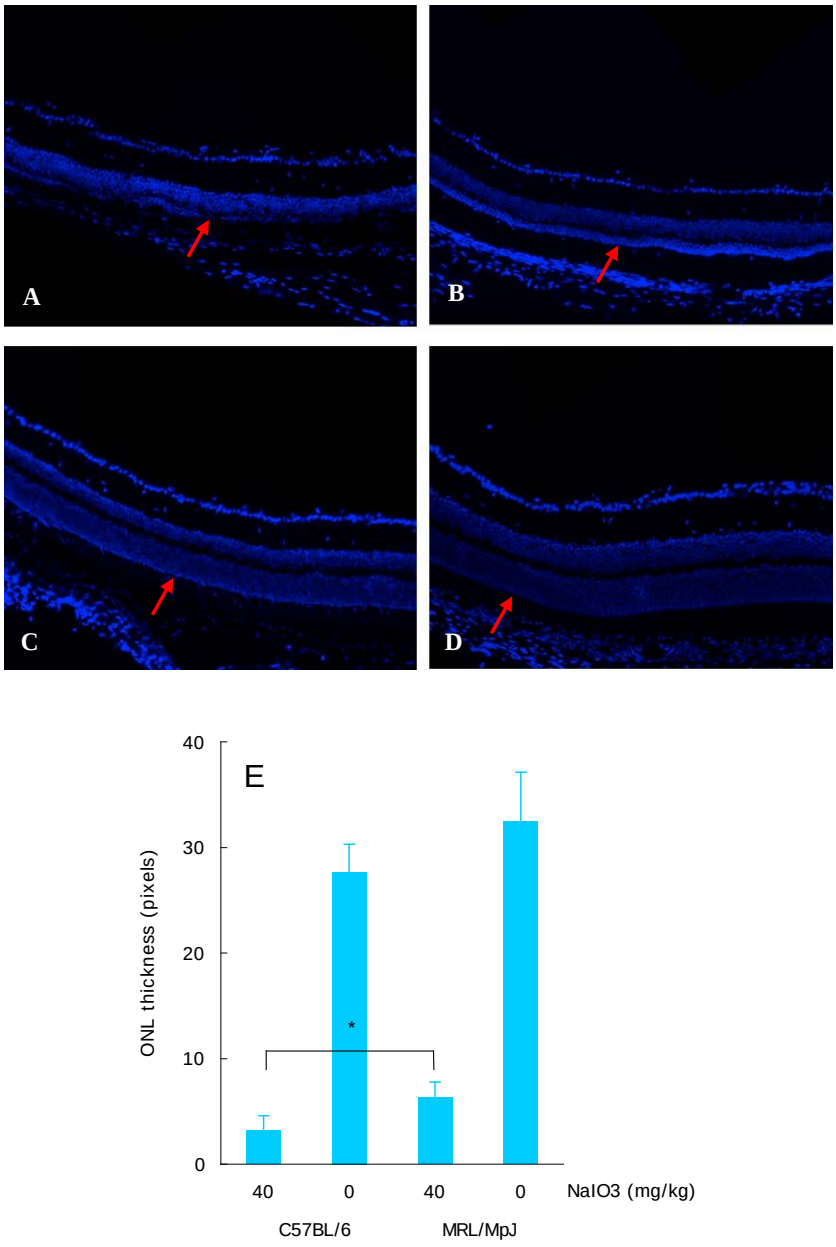

Figure 3-3. Comparison of ONL thickness between MRL/MpJ and C57/BL6 30 days post 40 mg/kg sodium iodate injection. A) C57/BL6 treated at 40mg/kg sodium iodate. B) MRL/MpJ treated at 40mg/kg sodium iodate C) C57BL/6 treated with PBS D) MRL/MpJ treated with PBS. E) Comparison of ONL thickness between the two strains after treatment (asterisk indicate P value less than 0.05, n≥3 for each group).

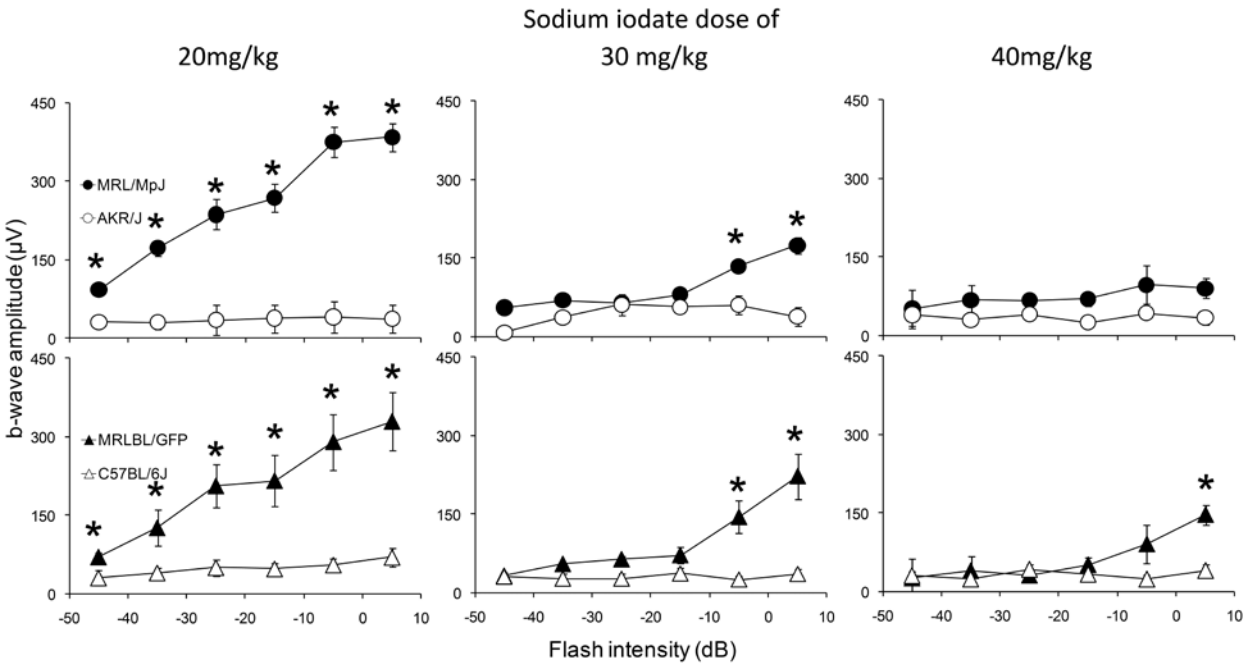

Figure 3-4. Comparison of b-wave amplitudes of MRL/MpJ and AKR/J, MRLBL/GFP and C57BL/6, at a dosage of 20, 30 and 40 mg sodium iodate/kg body weight 30 days post injection. ≥3 for each group. Significant level at $P<0.05$ is indicated by asterisks.

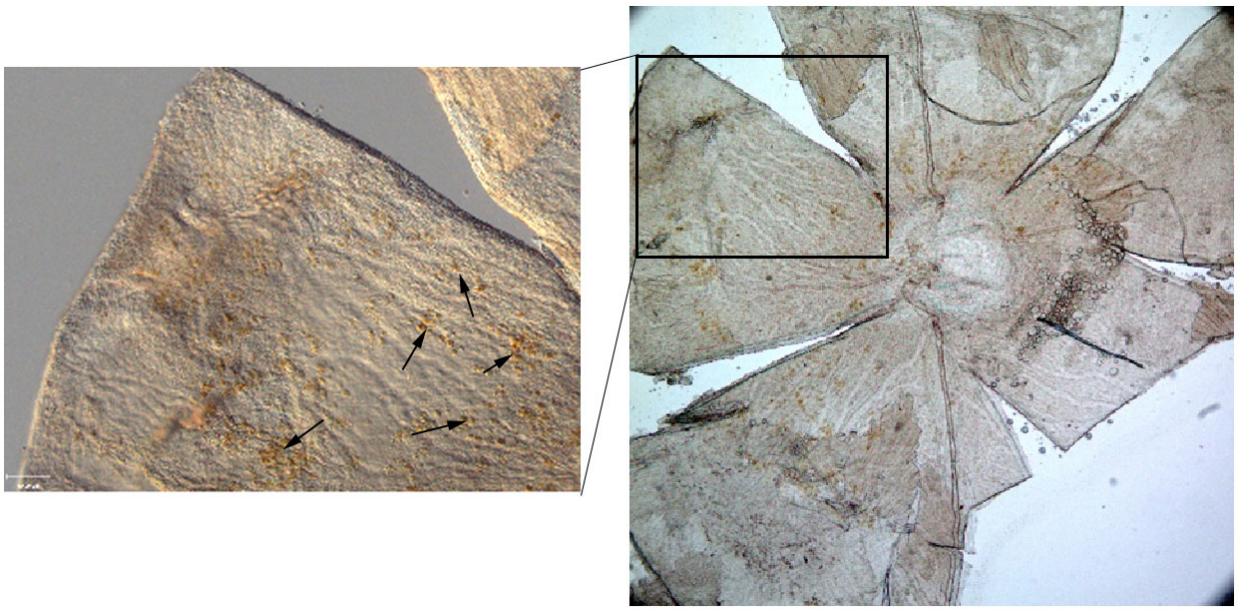

Figure 3-5. RPE cells that were considered to differentiated from donor CD133+ cells. Pigmented, RPE like cells (arrow) were observed on the flatmount of MRL/MpJ mice intra-vitreal injected CD133+ from MRL-GFP-Black.

CHAPTER 4
ENHANCED RETINAL PIGMENT EPITHELIUM REGENERATION AFTER INJURY IN MRL/MPJ MICE

It is not a simple task to prove “regeneration”. The one month single time point ERG difference after treatment is not sufficient to prove that MRL/MpJ mice have the ability to regenerate RPE regeneration. The difference can be explained as the “resistance” or due to the less damage at the first beginning. The difference will not be convincing until we provide evidence indicate that the RPE cells were damaged and lost after sodium iodate treatment, and after a period of regeneration, restored both “structurally” and “functionally”.

Time Course of ERG Response in MRL/MpJ Mice after Chemical Ablation of RPE

As established in the previous chapter, MRL/MpJ showed higher ERG responses than control strains at post-injection day 30. To follow the kinetics of the recovery process and to exclude the possibility that MRL/MpJ mice are more resistant to the initial injury, we monitored the ERG response in MRL/MpJ and AKR/J mice as a function of time after sodium iodate injection. Prior to treatment, both strains exhibited typical scotopic ERG responses characterized by a- and b-waves with superimposed oscillatory potentials (Figure 4-1). At early times after injection, both strains showed attenuated responses. At later times, the ERG response of MRL/MpJ mice was substantially restored, while that of AKR/J remained low (Figure 4-1). To account for strain differences in the pretreatment ERG response, we performed the analysis with ERG amplitudes normalized to the pretreatment values for the b-wave at -5 dB flash intensity. This analysis revealed nearly identical initial damage in both strains followed by recovery in MRL/MpJ but not AKR/J mice (Figure 4-2 A). Similar damage and recovery trends were observed with intensity-response data collected at flash intensities

from -45 dB to +5 dB (Figure 4-2 B). Statistical analysis of the -15 dB, -5 dB and +5 dB b-wave amplitudes at 5, 30 and 60 days post-injection with a mixed model statistical analysis indicated no significant difference in initial damage between the two strains (P=0.1214). Analysis at these stimulus intensities also indicated significant recovery in MRL/MpJ mice at 30 and 60 days compared to 5 days post-injection (P<0.0001 and <0.0001, respectively but not in AKR/J mice (P=0.4910 and 0.6258, respectively). These results suggested that MRL/MpJ and AKR/J mice are equally susceptible to sodium iodate injury, but only MRL/MpJ mice recover significantly. Thus, the increased ERG response in MRL/MpJ mice after sodium iodate treatment is not due to a greater resistance to the initial injury but rather to enhanced regeneration.

Loss and Restoration of RPE65 Expression in MRL Mice Posterior Cup after Injury

We conducted anti-RPE65 immunostaining to correlate the observed functional recovery with structural changes to the RPE in cryosections of posterior eyecups before and after sodium iodate injury. Prior to injury, immunohistochemical analysis with antibody against RPE65, an RPE-specific protein (90), revealed a thin, positively-stained band at the expected location between the neurosensory retina and the choroid (Figure 4-3 A and D). At higher magnification, polygonal RPE65-positive cells with large central nuclei characteristic of the RPE were clearly identifiable (Figure 4-3 G-L). RPE65 staining was dramatically reduced in both strains at 5 days post-injection (Figure 4-3 B and E). Strong central RPE65 staining reappeared at 30 days post-injection in MRL/MpJ but not AKR/J mice (Figure 4-3 C and E), consistent with the recovery of ERG responses (Figure 4-1 and Figure 4-2). The decrease in RPE65 staining following injury may be due to a reduction in the cellular expression of RPE65, a loss of RPE cells or

both. Measure and comparison of the ONL thickness of the stained cryosections of the eyes revealed a gradual thinning of ONL in the AKR/J strain but not obvious in MRL/MpJ mice (Figure 4-6). This may due to apoptosis of photoreceptor cells due to the lack of nourishing and supporting from the RPE cells. These results suggest that RPE cellular integrity was similarly disrupted by sodium iodate in both strains, but recovered more effectively in MRL/MpJ mice.

RPE Restructuring and Loss within Days of Sodium Iodate Injury

To further confirm the loss of RPE cellular integrity, we analyzed posterior eyecup preparations stained with rhodamine phalloidin, which detects filamentous actin (F-actin) on the apical border of RPE cells. Since conventional RPE/choroid/sclera flat mounts are subject to potential artifacts that arise when the adherent retina is removed, we examined eyecup whole mounts, in which the retina is retained. At two days following sodium iodate injection, both strains showed a similar extent of damage (Figure 4-4 A and B). Polygonal RPE cells were detected in the eyecup periphery, but were absent from the center, consistent with RPE cell atrophy and loss. The transition zone between healthy and atrophic tissue was characterized in both strains by irregularly-shaped RPE cells whose border curvature and area increased towards the eyecup center (Figure 4-4 A and B).

Visualization of the RPE in whole mount image stacks was challenging because of the abundance of F-actin and unevenness of tissue. Maximum merge z-projection of image stacks encompassing the RPE layer was typically uninterpretable (Figure 4-4 C). We therefore developed a “flattening” macro in ImageJ to extract the phalloidin-stained RPE cell borders (Figure 4-4 D) and generate an image containing the RPE apical surface in a single plane (Figure 4-4 E). These images clearly revealed structures

reminiscent of RPE cellular shedding events within the transition zone of sodium iodate-injured mice in both AKR/J and MRL/MpJ (Figure 4-4 E, asterisks). Taken together, these results establish that sodium iodate treatment at 20 mg/kg body weight produces a gradient of RPE loss and cellular tissue restructuring that is similar in both strains.

Enhanced Restoration of RPE Morphology at One Month

In order to better characterize the loss and regeneration of RPE in the MRL and control animals we examined phalloidin-stained posterior eyecup whole mounts at one month post-injection (Figure 4-5). Mosaic images of AKR/J and MRL/MpJ mice were generated starting at the superior, periphery and ending at the optic nerve head. AKR/J mice at one month post-injection retained extensive areas toward the optic nerve head that were completely devoid of polygonal RPE cells as detected by phalloidin staining (Figure 4-5 A and B). By comparison, and in contrast to the appearance at two days post-injection, phalloidin staining of MRL/MpJ eyecups at one month post-injection showed the polygonal RPE cells throughout the posterior eye (Figure 4-5 C and D), a striking improvement to the disrupted morphology observed at two days post-injection. The large, irregularly-shaped cells observed at early times after injury (Figure 4-4 A) were mostly absent. Polygonal cells were observed mainly in the periphery of AKR/J eyes, which might contribute to the small amount of ERG recovery in the AKR/J strain (Figure 3-4, Figure 4-1, Figure 4-2). Phalloidin-stained F-actin structures reminiscent of those in fibroblasts were observed at the transition between the normal and atrophic RPE, suggestive of scar formation. These results demonstrate that the RPE region damaged by sodium iodate can be efficiently regenerated in MRL/MpJ but not AKR/J mice.

Confirmation of Morphological Changes in Plastic Embedded Sections

To confirm the post injury morphological changes, ultra-thin plastic embedded sections were prepared at day 0, 5 and 30 post-injection. The images revealed severe central RPE damage at 5 days post injection in both MRL/MpJ and AKR/J mice (Figure 4-7, arrowheads). At 30 days post injection, the typical structure of the RPE layer was restored in MRL/MpJ mice but not in AKR/J mice (Figure 4-7, arrows). At 30 days, the outer nuclear layer and photoreceptor inner and outer segment were largely preserved in MRL/MpJ mice consistent with a restoration of RPE function. These results further confirmed RPE65 and phalloidin staining result suggesting that the MRL/MpJ mice were able to regenerate RPE efficiently after sodium iodate injury.

Cell Proliferation

To test if cell proliferation contributes to the observed RPE regeneration, BrdU was injected daily following sodium iodate treatment. At 30 days post injection, many BrdU positive cells were observed in the subretinal space of sodium iodate treated MRL/MpJ mice (Figure 4-8 D and H) but only sporadically in AKR/J mice (Figure 4-8 B and F). Some of these cells have large nuclei and located in a monolayer above Bruch's membrane, suggesting they are RPE cells. BrdU incorporation was not observed in uninjured mice (Figure 4-8 A, B, E and F) indicating that incorporation reflects a post injury proliferation. These results suggest that after injury, there are proliferating cells in the subretinal space in MRL/MpJ mice but not AKR/J mice that may contribute to the regeneration of the RPE.

In this chapter, we investigated RPE recovery in MRL/MpJ mice after sodium iodate treatment. Electroretinography and BrdU labeling and histology was performed to assess RPE damage and restoration in MRL/MpJ and control strains. We found that

MRL/MpJ mice show more robust structural and functional regeneration than control mice after injury with a full recovery of ERG responsiveness. Our result provides the first demonstration of enhanced RPE regeneration in rodents and provides a significant new tool for future studies of RPE regenerative therapy.

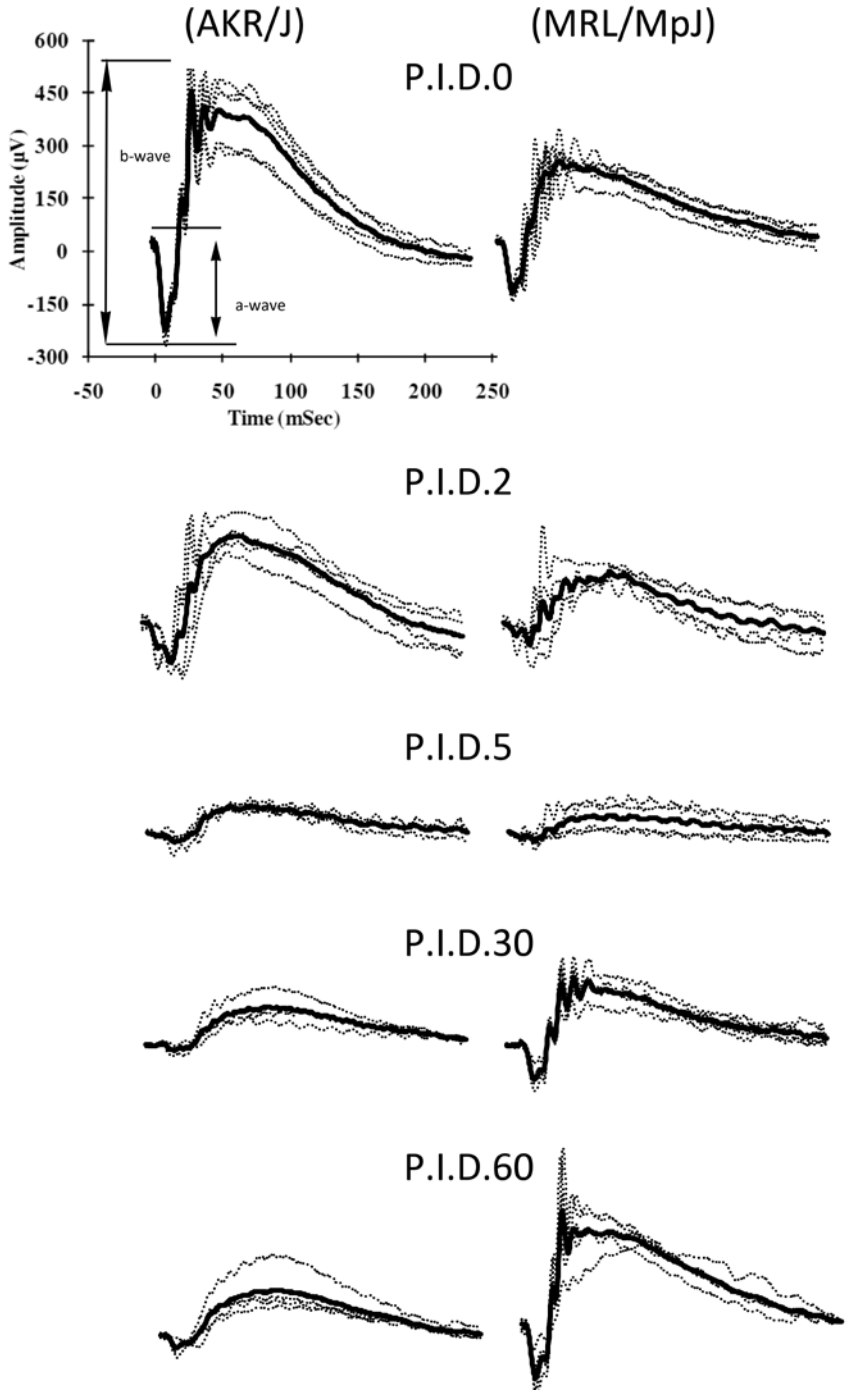

Figure 4-1. Single and average ERG traces at -5dB intensity. ERG traces in MRL/MpJ and AKR/J mice at an intensity of -5 dB were recorded at 0, 2, 5, 30 and 60 days after sodium iodate injection. Thick line:mean ERG response. Thin line:individual traces. n≥3 for each group.

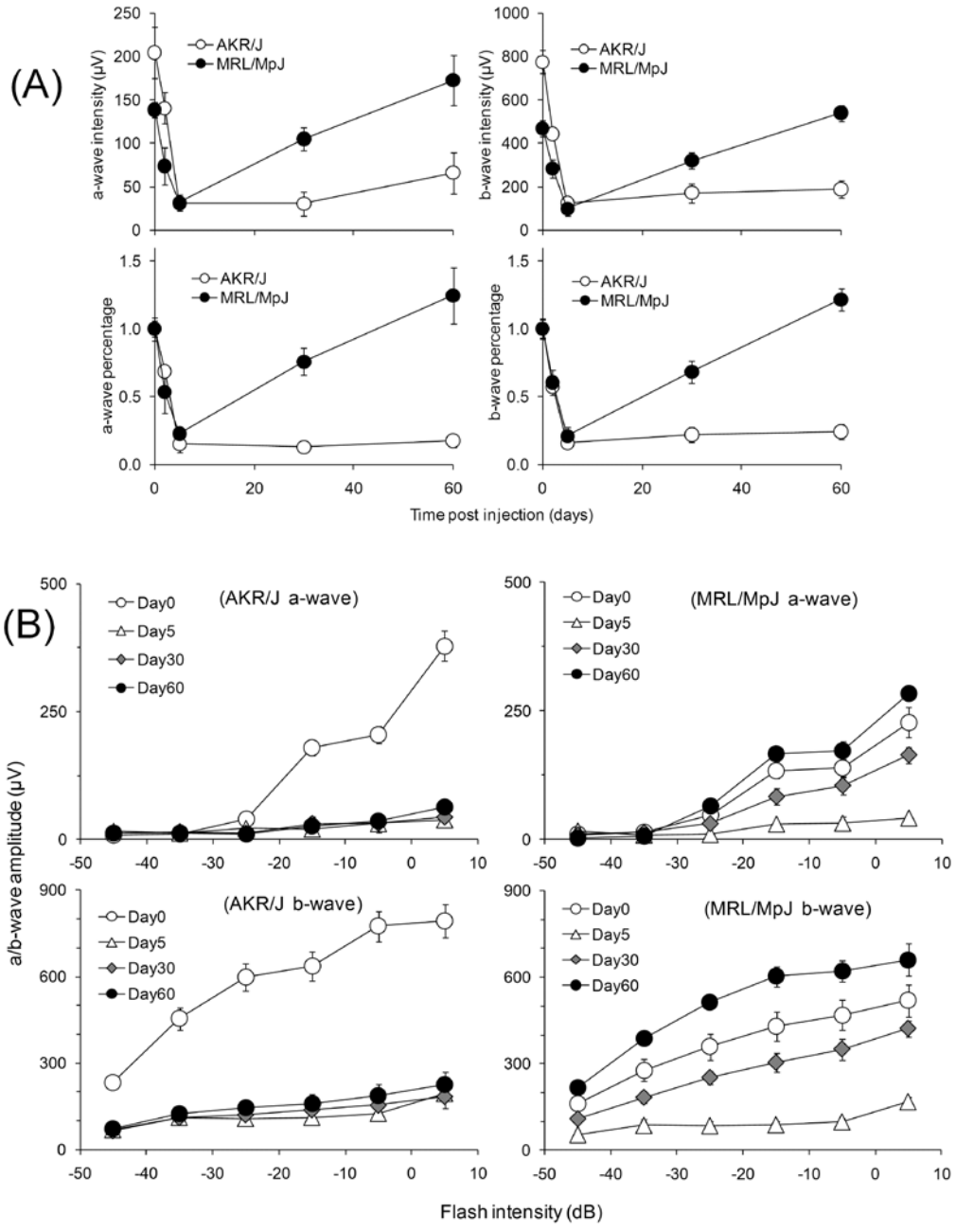

Figure 4-2. Analysis of ERG a- and b- wave amplitude under different flash intensity. A) Respective time based a- and b-wave amplitude and percentage analysis at -5 db. B) Flash dose dependent response of AKR/J and MRL/MpJ at different time points after sodium iodate treatment. n≥3.

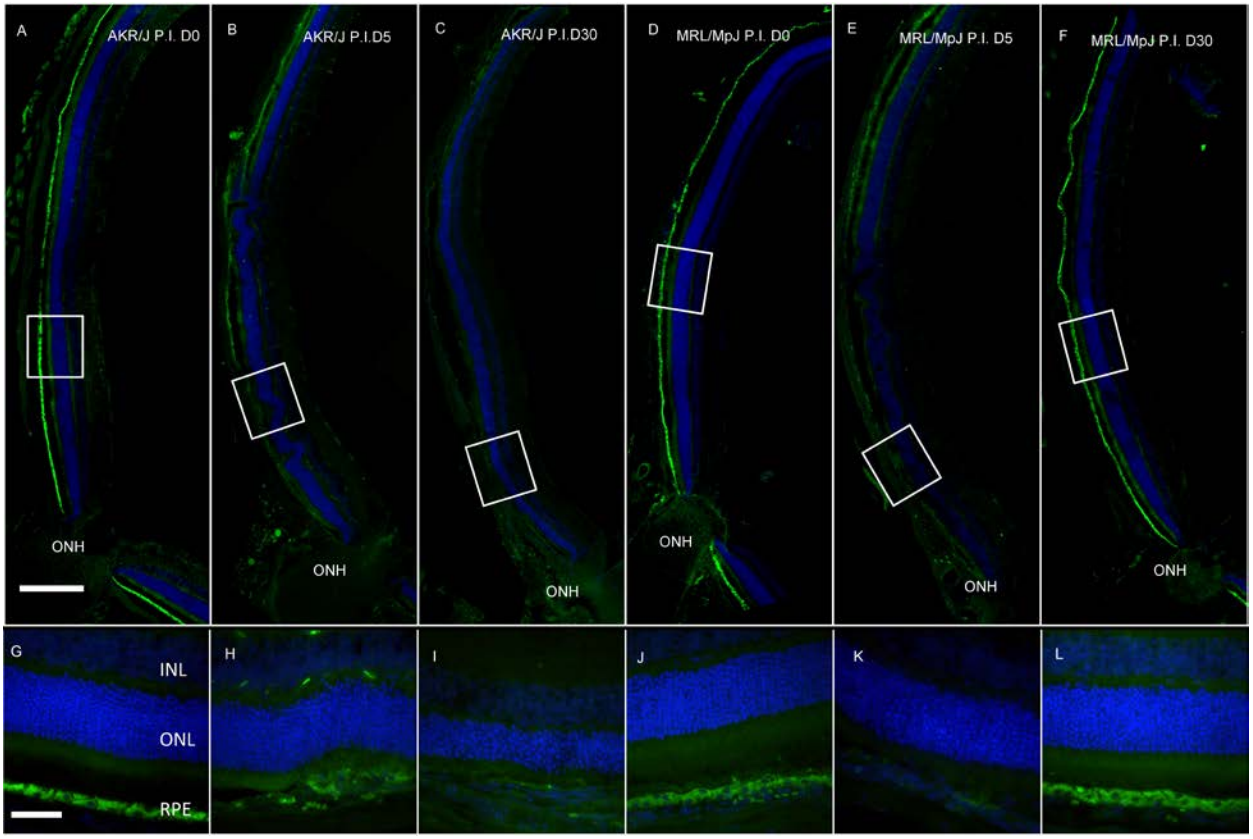

Figure 4-3. Immunostaining of RPE65 in cryosections of MRL/MpJ and AKR/J 30 days post injection. A-C) Fluorescence micrographs of posterior cup cyosections of AKR/J. D-F) Fluorescence micrographs of posterior cup cyosections of MRL/MpJ. G-L) High magnification view of A-F. Scale bar A-F: 200 µm; G-L:50 µm. ONH: optic nerve head. Green: AlexaFluor 488; Blue: 4'-6-diamidino-2-phenylindole (DAPI).

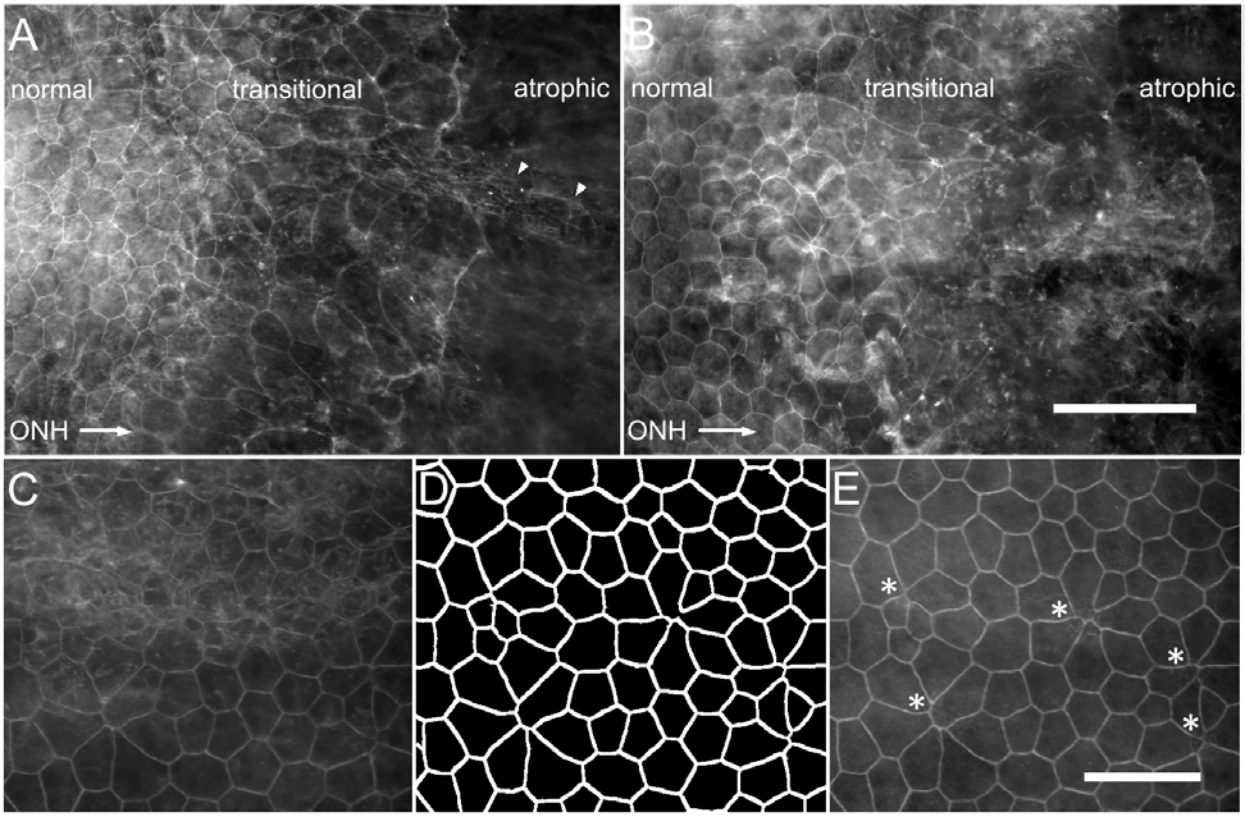

Figure 4-4. Mosaic image of posterior eyecup whole mounts stained with rhodamine phalloidin. A) AKR/J. B) MRL/MpJ. C-E) The transitional zone examined at higher magnification. Asterisks, RPE apical surface and possible shedding events within the transitional zone. Scale bars: A and B, 100 µm; C-E, 50 µm. ONH: optic nerve head.

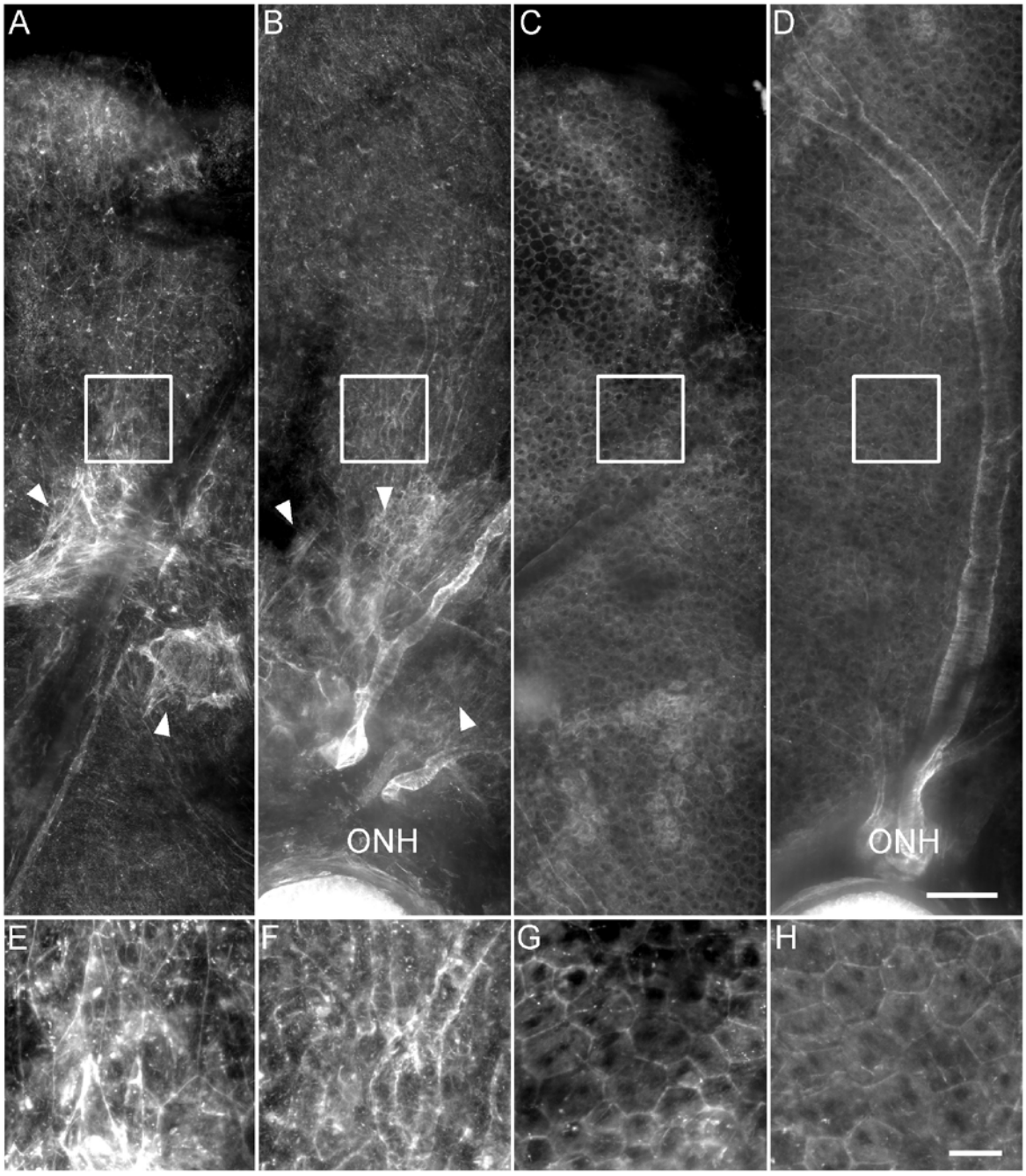

Figure 4-5. Whole mounts of MRL/MpJ and AKR/J stained with rhodamine-phalloidin. A-B) Superior and central whole mounts of AKR/J. C-D) Superior and central whole mounts of MRL/MpJ. E-H) Higher magnitude view of box area in A-D. ONH: optic nerve head. Scale bars: A-D, 100 μm; E-H, 25 μm.

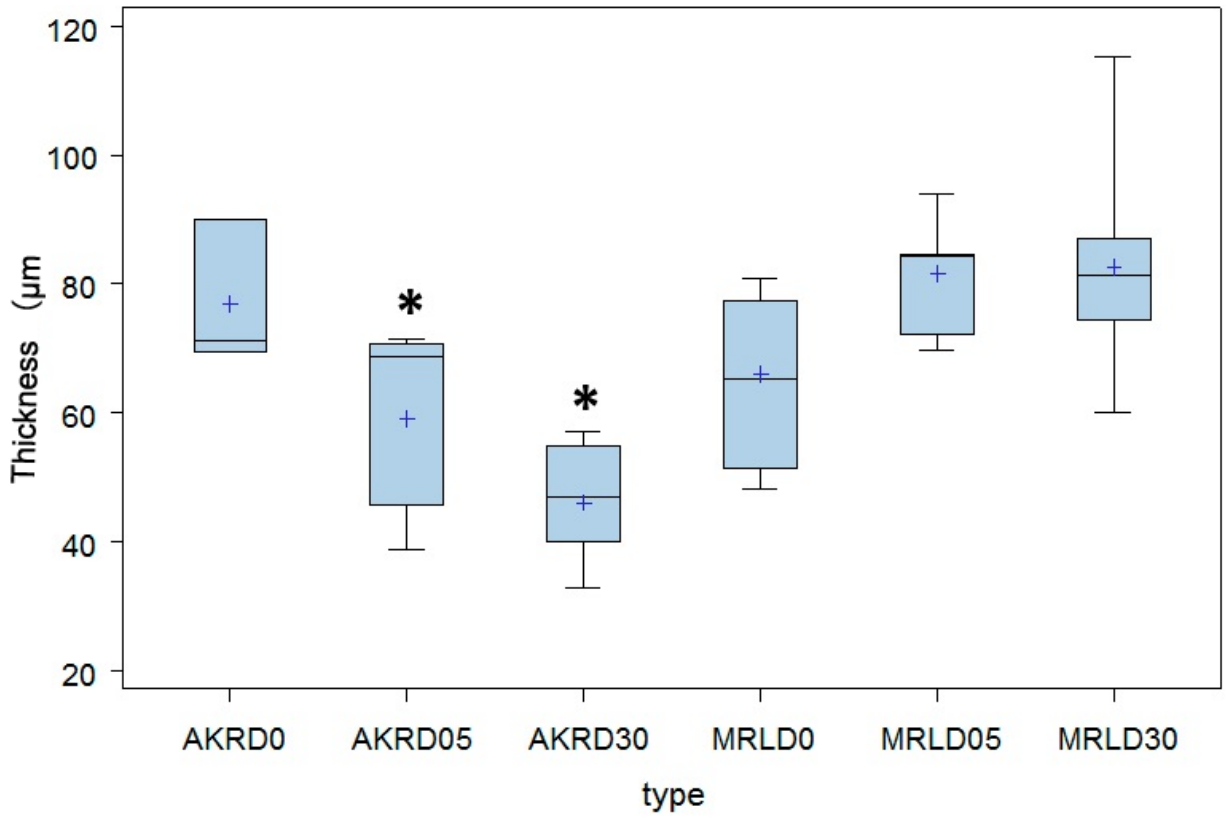

Figure 4-6. Measurement of outer nuclear thickness (ONL) after 20mg/kg sodium iodate injury. The thickness of ONL in the immunostained cryosections of posterior cup was measured and compared at different time point after 20 mg/kg sodium iodate injection. ANOVA analysis and simultaneous comparison between the tissues collected different time point and different strains indicate the ONL become thinner suggesting some degeneration process taking place.

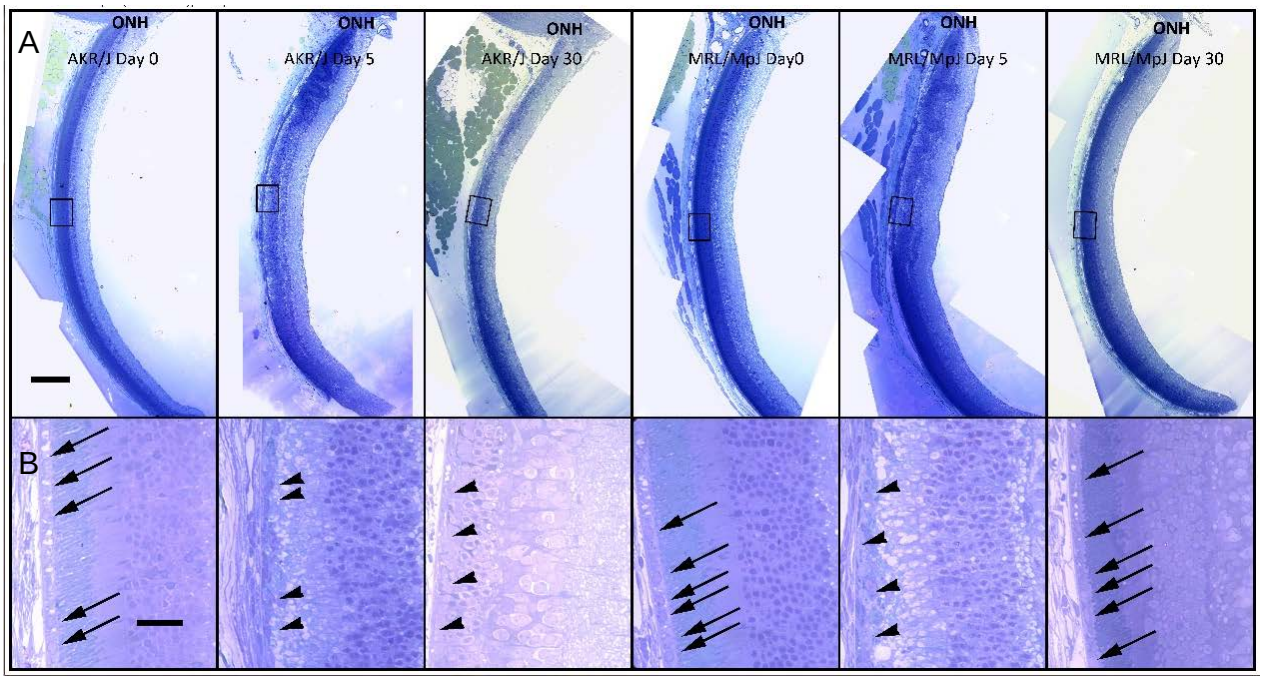

Figure 4-7. Comparison of RPE integrity in plastic embedding sectioning of MRL/MpJ and AKR/J after sodium iodate injury. A) Bright field images of plastic-embedded eyecups. B) Higher magnitude view of panel A. Scale bars: upper panel 200 µm; lower panel 50 µm. ONH: optic nerve head. Arrows: healthy RPE layer. Arrow heads: damaged RPE layer.

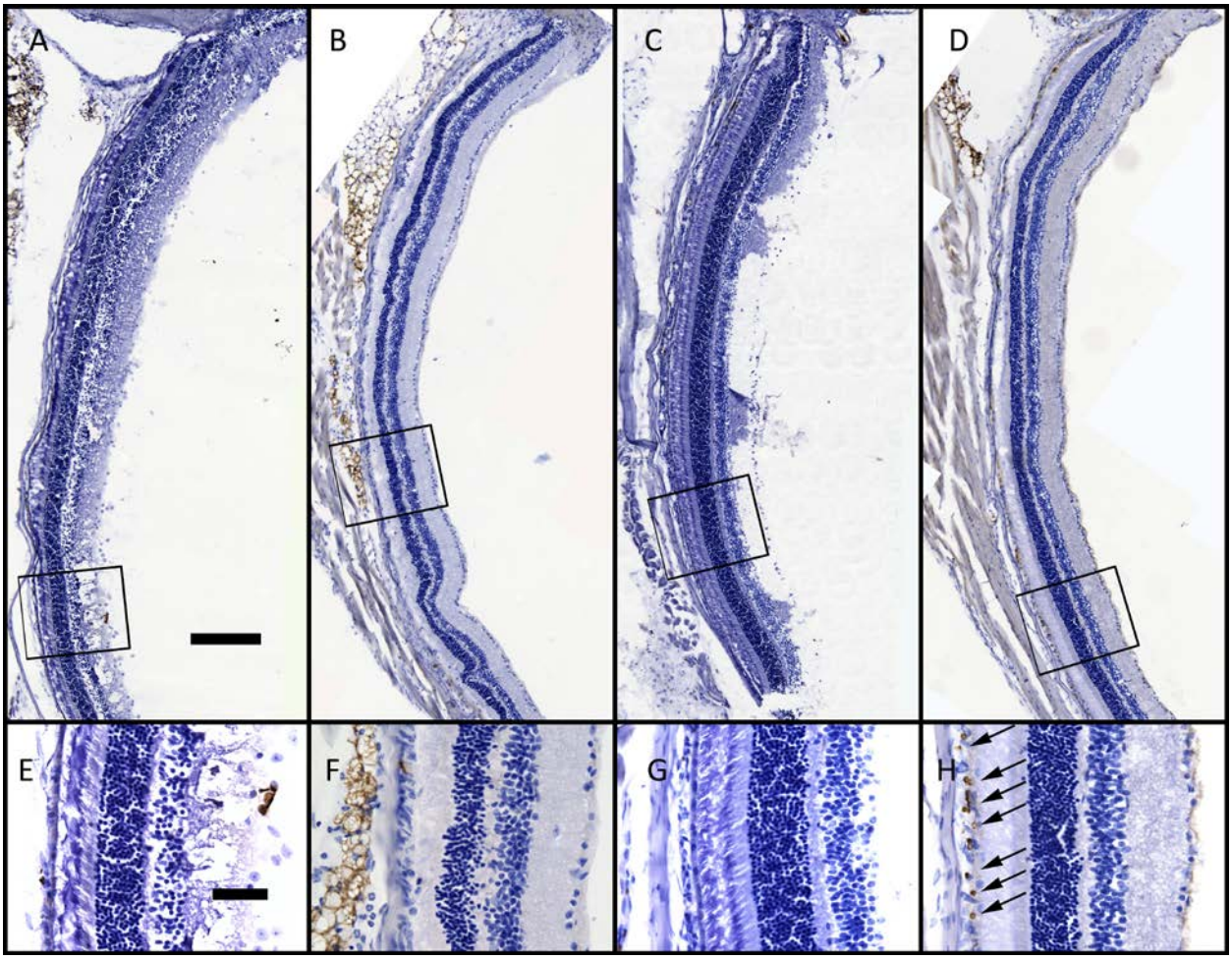

Figure 4-8. Observation of cell proliferation by BrdU staining. A) Bright field pictures of eye sections from AKR/J mice treated with PBS. B) Bright field pictures of eye sections from AKR/J mice treated with 20 mg/kg sodium iodate. C) Bright field pictures of eye sections from MRL/MpJ mice treated with PBS. D) Bright field pictures of eye sections from MRL/MpJ mice treated with 20 mg/kg. E-H) Higher magnitude picture of the boxed area of panel A-D. BrdU positive cells (arrows), Scale bars: A-D, 200 μm; E-H, 50 μm.

CHAPTER 5
INVESTIGATION OF REGENERATION MECHANISM

We have established the RPE regeneration ability in the MRL/MpJ mice in the previous chapter. In this chapter, possible regeneration mechanisms were investigated. Modifications by whole bone marrow transplantation were conducted aiming to reproduce the regeneration in the normal genetic background.

Introduction of p21 K.O. Mice as Another Regeneration Strain

Due to the genetic complex of the natural mutant strain MRL/MpJ, investigation of the regeneration mechanism will be continued in this chapter with the single gene knockout strain- B6.129S6(Cg)-Cdkn1a^{tm1Led}/J (p21 K.O). Compared to the MRL/MpJ mice, the p21 K.O. strain has at least three advantages: 1) it is a single gene knock out strain of B6 mice so the genetic background is well documented; 2) unlike MRL/MpJ, the p21 K.O. strain will not develop any auto-immune disease; 3) it has k-halplotype, which is the same as C57BL/6 so that the bone marrow transplantation is compatible with C57BL/6 and most of the other strains. The first question we have to ask is does p21 K.O. mouse able to regenerate tissues other than the ear and heart, especially RPE? Due to the fact that the regeneration is highly tissue-specific, we have to re-examine the RPE regeneration ability of p21 K.O. mice. We treat the C57BL/6, MRL/MpJ and p21 K.O. mice with 20mg/kg sodium iodate. We found that the p21 K.O. mice can restore the ERG response more like a MRL/MpJ mice and clearly different from its parent strain C57BL/6 (Figure 5-1).

Comparison of Gene Expression in the Posterior Cup

The fundamental question in this chapter is to ask what are the factors that may contribute to the RPE regeneration. Generally speaking, the factors can be classified as “local environmental factors” and “circulating stem cells”. We want to compare the differences in each aspect. To compare the local gene expression difference, we examined the gene expression profile in the posterior cups of different strains at five days post injection, a time point we believe the regeneration start. By the reported candidate genes involved in the regeneration of other tissues in MRL/MpJ mice, Axolotl and zebrafish (63, 82, 91), we choose MMP-2, MMP-9, TGFβ-1, TGFβ-2, TGFβ-3 and Plk-1 as candidates. Five days post sodium iodate injection, the posterior eye cups were collected, homogenized and RNA extracted. The cDNA were synthesized by reverse transcriptase. Real-time reverse transcript PCR was conducted in triplicate with the primers recognizing murine MM-2, MMP-9, TGFβ-1, TGFβ-2, TGFβ-3 and Plk-1 cDNAs with beta-actin as an internal standard. The expression levels were compared as shown in Figure 5-2. We find that the relative expression level of TGFβ-3, MMP-2, MMP-9 and Plk-1 were significantly higher in MRL/MpJ mice after sodium iodate injection. This result may indicate that the reduced scarring (TGFβ-3,), increased permeability and enhanced cell proliferation that contribute to the regeneration.

Comparison of Circulating Stem Cell and Bone Marrow Cell Difference

Accumulating evidence suggested that the bone marrow derived cells can contribute to the replenishing of RPE cell loss (51, 92). As a result, we asked is there any difference with the circulating hematopoietic stem cells or the bone marrow cells

between the regeneration strains and non-regeneration strains. The hypothesis is that a more immature bone marrow or circulating stem cell may be account for the enhanced regeneration ability, immature in terms of there are more stem/progenitor cells within the circulating system and the bone marrow. By using FACS system, we checked the percentage of stem cell/lineage marker positive cells. We found that in MRL/MpJ mice, the fraction of CD117+ cells, one of stem cell markers, were larger when compared to the control group (Figure 5-2). This discovery is consistent with the fact that populations of cells expressing the embryonic stem cells markers of are retained as well as number of embryonic metabolism features(71).

Whole Bone Marrow Cross Transplantation

As from the previous experiment, it is suggested that that circulating/bone marrow cells were different between the regenerative and non-regenerative strains. It will be not so convincing until we can provide the evidence that the change of the circulating/bone marrow cells will also change the regenerative ability. To achieve that, after sodium iodate treatment, p21 K.O. and C57BL/6 mice were irradiated and under whole bone marrow transplantation with bone marrow cells from either the p21 K.O. or the C57BL/6 mice forming four cohorts of chimeric mice. After one month period of recovery, the ERG response of each cohort was measured and compared (Figure 5-4). We find that the ERG response was higher in the cohorts transplanted with the p21 K.O. bone marrow cells than those transplanted with C57BL/6 bone marrow cells. Moreover, p21 K.O. host transplanted with C57BL/6 donor showed no significant advantage over the cohorts with C57BL/6 host and C57BL/6 donor. However, cohorts with p21 K.O. host transplanted with p21 K.O. donor did show better regeneration ability over the cohorts with C57BL/6 host and p21 K.O. donor indicating the contribution by the host

background. Analysis of the flatmount of posterior cup of the chimera mice (host/donor) also yield similar conclusion: (p21 K.O.)/(p21 K.O.) chimera has the healthiest look RPE layers and (C57BL/6)/(C57BL/6) has the worst; (C57BL/6)/(p21 K.O.) has better RPE integrity than the (p21 K.O.)/(C57BL6) (Figure 5-5). It might be reasonable to predict that there might be some synergetic effect between the circulating stem cell and the micro-environment.

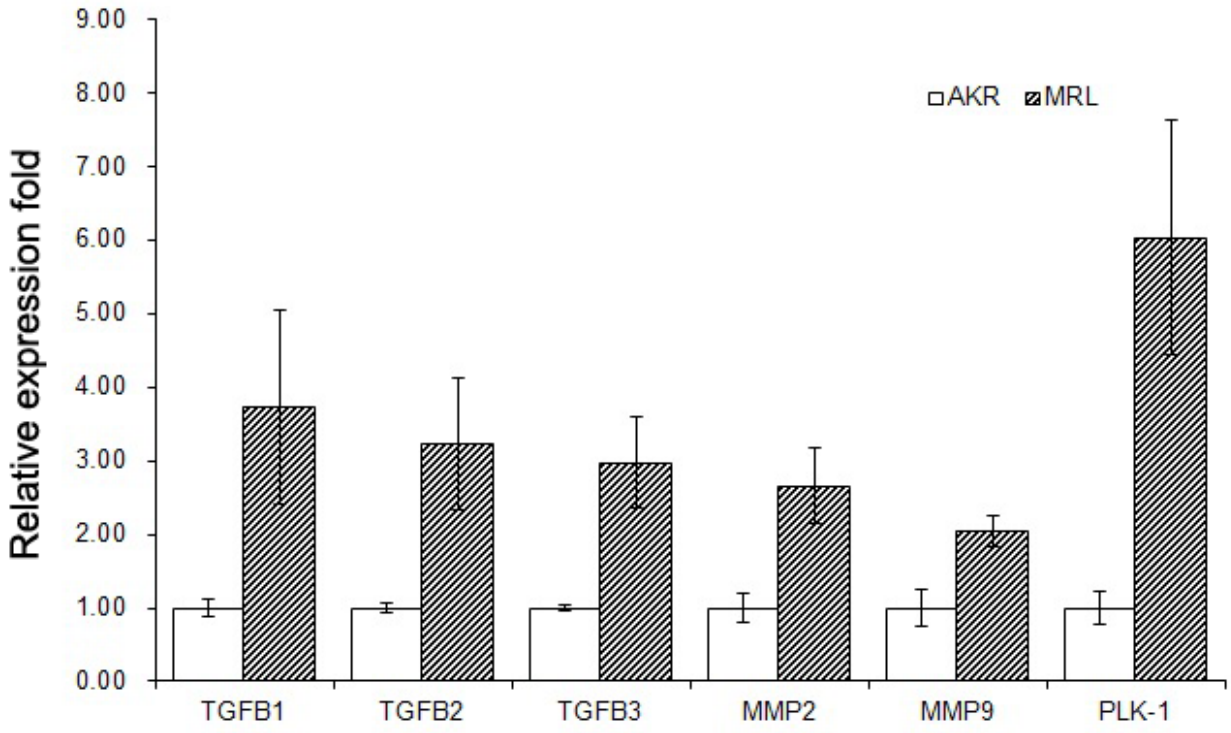

Figure 5-1. Real-time reverse transcript PCR analysis of gene expression profile difference between different strains in the posterior cup 5 days post injection. The expression level of each gene is normalized to that of β-actin. The expression level in MRL/MpJ mice is then normalized by the average of the expression level in the control conhorts.

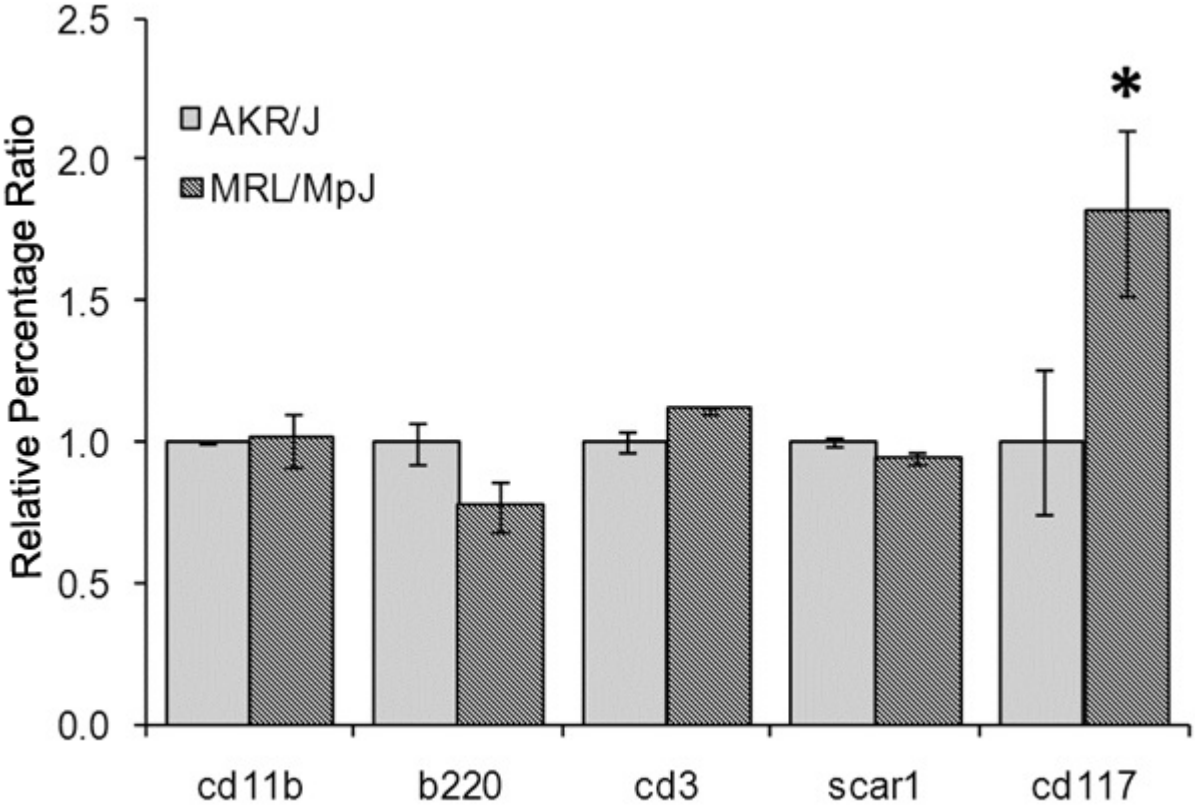

Figure 5-2. FACS analysis of peripheral cell difference in MRL/MpJ and AKR/J 5 days post sodium iodate injection. The collected peripheral blood samples from MRL/MpJ and AKR/J were stained with various FITC conjugated antibodies and analyzed by FACS. The percentage of each cell population in MRL/MpJ mice were normalized by the average of the percentage in AKR/J mice. n≥3.

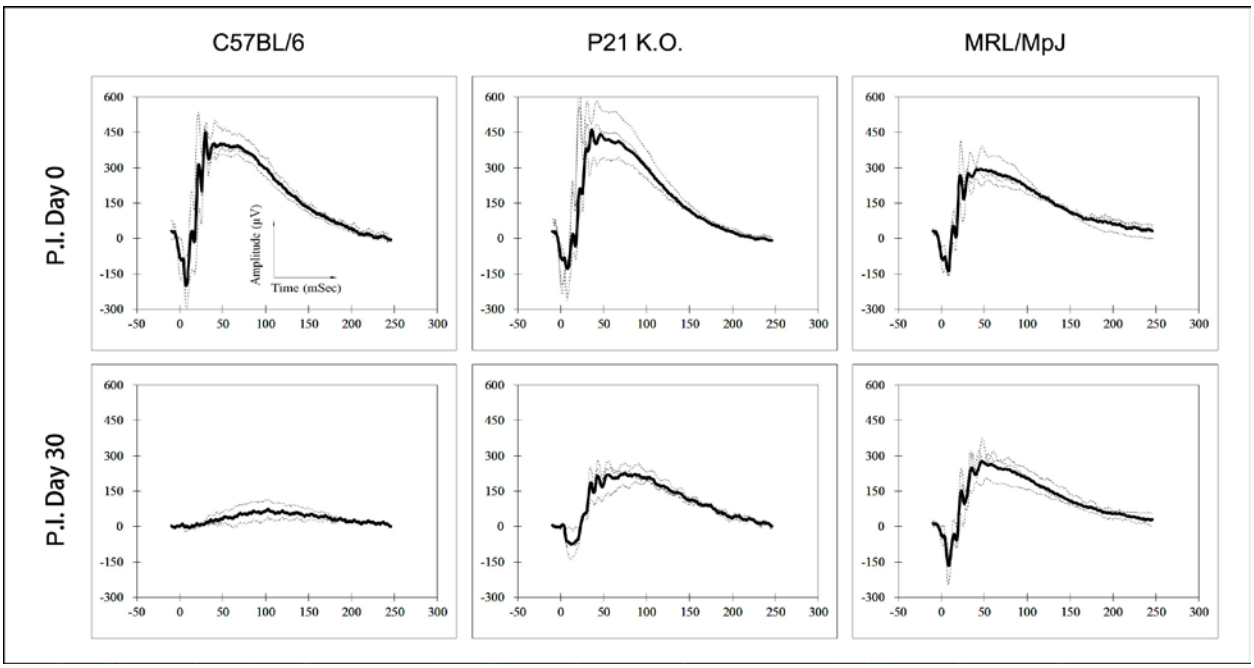

Figure 5-3. ERG analysis of C57BL/6, p21 K.O. and MRL/MpJ mice post sodium iodate injection recovery. C57BL/6, p21 K.O. and MRL/MpJ mice were treated with 20mg/kg body weight. The ERG responses were recorded before and 30 days post injection.

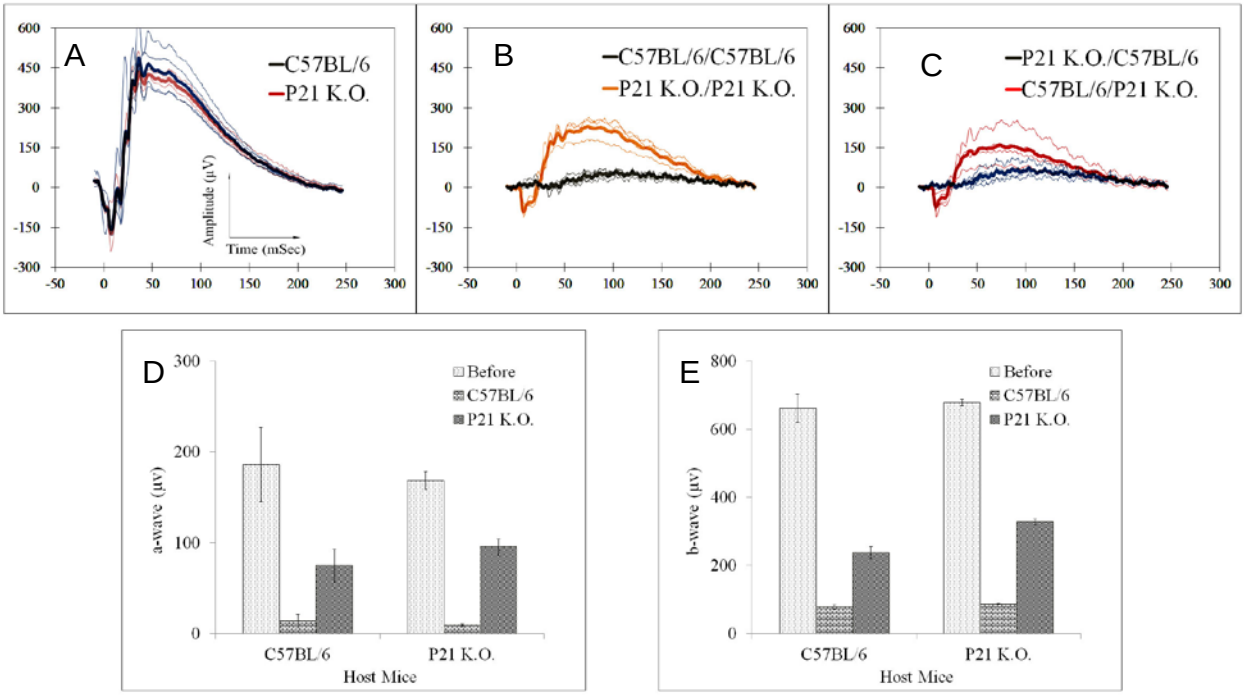

Figure 5-4. ERG analysis of cross bone marrow transplanted chimeric mice before and 30 days after treated with 20 mg/kg sodium iodate. A) Comparison of C57BL/6 and p21 K.O. before bone marrow transplantation. B) C57BL/6 and p21 K.O. mice treated with 20 mg/kg sodium iodate and self-MBT. C) C57BL/6 and p21 K.O. mice treated with 20 mg/kg sodium iodate and cross-MBT. D) a-wave analysis of A), B) and C). E) b-wave analysis of A), B) and C).

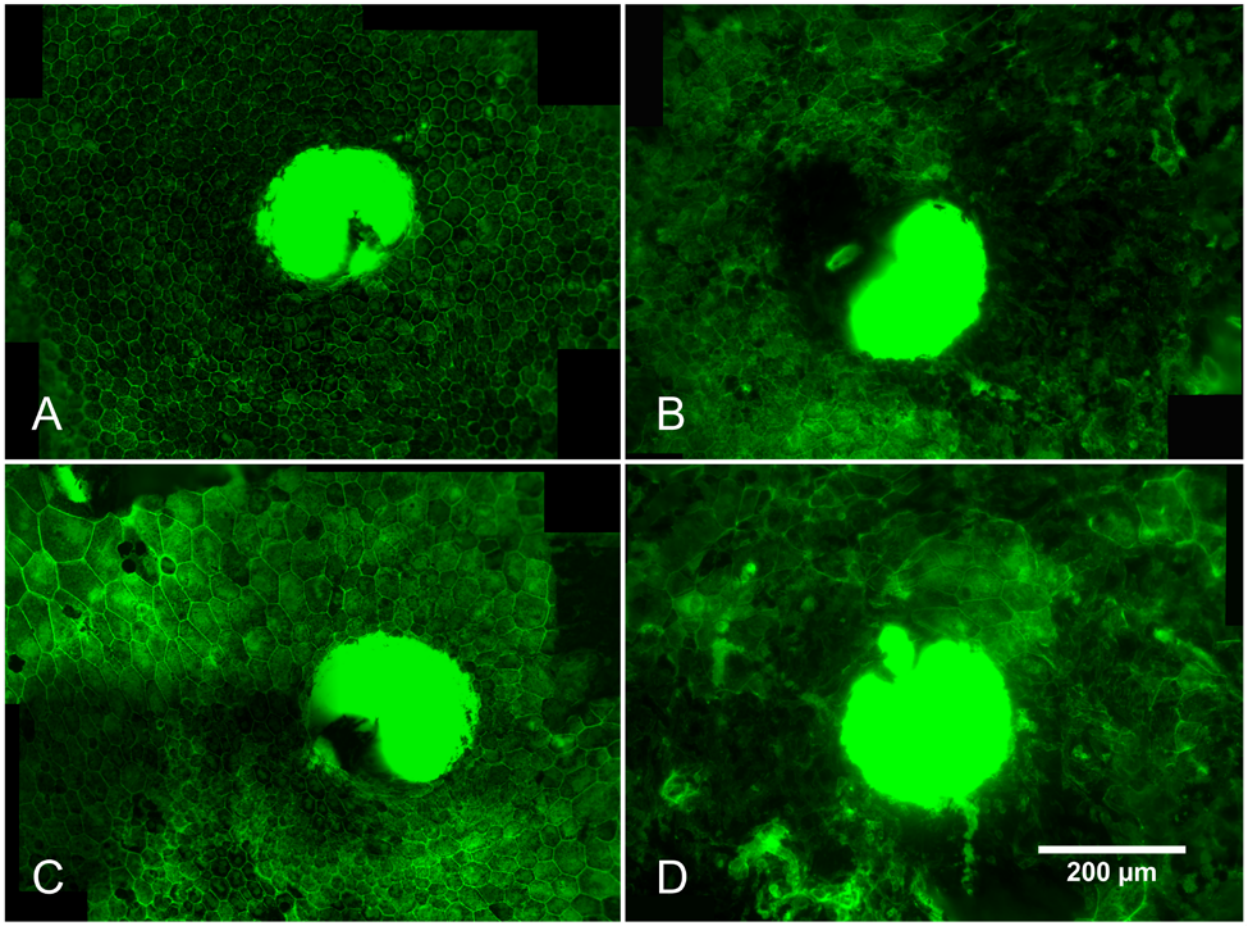

Figure 5-5. Flatmount of bone marrow transplanted cohorts stained with FITC-phalloidin. We will annoted the chimera mice as (Host)/(Donor). The chimeras were treated with 20 mg/kg sodium iodate prior bone marrow transplantation. The posterior cups were harvested 30 days post injection. A) Flatmount (p21 K.O.)/(p21 K.O.). B) (p21 K.O.)/(C57BL6/J). C) (C57BL6/J)/(p21 K.O.). D) (C57BL6/J)/(C57BL6/J).

CHAPTER 6
DISCUSSION AND CONCLUSION

Our group has previously showed the bone marrow derived progenitor cells can be differentiated into RPE cells (51, 54) with low efficiency. The goal of the current work is to identify a mouse model with robust regeneration of RPE in response to injury that can be used in future studies to elucidate the underlying pathways. Our analysis indicates that RPE regeneration after sodium iodate injury is significantly enhanced in MRL/MpJ mice compared to AKR/J mice. We identified a sodium iodate dose of 20 mg/kg under which a clear difference in recovery was observed between these strains. At this dose, the ERG response at 60 days after damage in MRL/MpJ recovered beyond pretreatment amplitudes, consistent with a more than sufficient restoration of RPE function, which is essential for photoreceptor viability and activity (12). By monitoring tissue histology and morphology as a function of time after sodium iodate injury, we demonstrated that the RPE of both strains undergoes similar cellular damage after injury, but only MRL/MpJ recovers significantly. BrdU incorporation studies indicate that MRL/MpJ recovery correlates with an increased labeling of subretinal nuclei, consistent with a contribution of cell division to regeneration in this MRL/MpJ tissue. The loss and subsequent recovery of RPE function and structure in MRL/MpJ mice satisfies the criteria of a regenerative process (34).

A modest level of sodium iodate-induced injury appears to be critical for detecting RPE regeneration in rodents. Although published studies are difficult to compare because of differences in the sodium iodate dose, mode of administration, age of animals and time of analysis after injection, major trends can be identified. Complete RPE ablation in mice is often achieved with sodium iodate at 40 – 100 mg/kg body

weight injected intravenously or intraperitoneally. Under these conditions, little (93) to no (89, 94, 95) regeneration has been found. We observed a similarly low level of regeneration in MRL/MpJ and control mice, including pigmented strains, with retro-orbital sodium iodate at 40 mg/kg body weight, in agreement with our previous work (51, 54). By contrast, significant regeneration has been suggested to occur at lower doses. For example, intravenous sodium iodate in C57BL/6 mice at 15 and 25 mg/kg body weight caused a dip and subsequent partial recovery of visual function as measured by a sensitive optomotor kinetic reflex assay, possibly indicating RPE regeneration (60). Consistent with these studies, we found robust regeneration of MRL/MpJ RPE with retro-orbital sodium iodate at 20 mg/kg body weight. The importance of a lower dose may reflect a need to preserve adult RPE cells or tissue-resident stem cells that repopulate the damaged tissue. Alternatively, high doses may damage circulating stem cells required for regeneration, as suggested previously (51); alter the tissue microenvironment so that it no longer supports RPE regeneration; or induce secondary damage due to inflammatory responses, as suggested as an explanation for RPE cell loss in a genetic ablation model (96). The observed dependence of regeneration on the severity of sodium iodate injury fits with the variable outcomes of tissue regeneration in MRL/MpJ mice (65, 67, 97-106).

Unlike reports of patchy RPE loss in response to a low sodium iodate dose (60, 94), our results indicate contiguous damage of the central posterior RPE with preservation of the periphery. We did not observe patches of RPE cell loss in the strains we examined, possibly because we avoided damage to the RPE by examining whole eyecup preparations in which the retina remained intact. In earlier attempts where the

retina was removed, we found that adherence of the RPE and retina introduced artifacts that made it difficult to interpret changes in RPE morphology, especially in sodium iodate-injured eyes. The loss of central RPE with peripheral preservation with low sodium iodate doses has also been reported in C57BL/6 mice (95) and rabbits (107). Greater central damage has also been noted at higher sodium iodate doses in mice (89, 93) and rats (93), and is supported by fluorescein angiography in rabbits and monkeys, which reveal a sodium iodate-induced breakdown of RPE barrier function in the central eye early after injury (108). Since major blood vessels of the choroidal and retinal circulation enter and exit the central eye at the optic nerve and have their largest diameter there, we speculate that delivery of and damage from sodium iodate is greatest in this region. However, it is also possible that damage is uniform throughout the eye, but peripheral regions are repaired more rapidly due to the presence of progenitor or stem cells in these regions (109).

Features of the transition zone between normal and atrophic RPE in MRL/MpJ and AKR/J mice reveal a similar initial response to sodium iodate injury in both strains. Flower-like cell shedding structures in the transition zone have previously been observed in chick embryonic RPE (110), in transgenic mice following genetic ablation of the RPE (96), and in cell culture models of epithelial shedding (111, 112). RPE shedding structures are associated with apical ejection of a central dead or dying RPE cell (110). Enlarged cells with irregular borders at the central edge of the transition zone may be similar to those reported at the boundary of RPE atrophy in retinal cross sections and in RPE/choroid/sclera flat mounts of sodium iodate-injured mouse and rabbit eyes (113, 114). These observations lead us to propose an initial injury response

in which dead or dying RPE cells are shed by a “purse string” closure process characteristic of epithelial monolayers (115). Neighboring cells rearrange to cover the area occupied by the shed cells, as suggested in a genetic RPE ablation model (96), resulting in enlarged cells with irregular boundaries. In the face of continued atrophy, RPE cells at the edge of the transition zone dedifferentiate, losing their characteristic polygonal shape and RPE65 expression. Further studies may reveal whether the RPE is repopulated in sodium iodate-injured MRL/MpJ mice by proliferation of cells at the central edge of the transition zone.

The establishment of enhanced RPE regeneration in MRL/MpJ mice is an important first step towards identifying factors that may improve regenerative approaches for age-related macular degeneration and related diseases. MRL/MpJ mice are not universal “healer” mice as they were originally nicknamed (101-106), and even the original ear-punch regeneration phenotype has been observed at much lower levels in other strains, including C57BL/6 (116, 117). Nevertheless, there is general agreement that tissue regeneration is most robust in MRL/MpJ strain, making it the most experimentally tractable for studying this process. In many ways the fact that MRL/MpJ mice are nearly normal makes them a potentially more relevant model for regenerative studies, as long as the tissue of interest is repaired in this background. Our results clearly show full restoration of ERG function in MRL/MpJ mice following acute sodium iodate injury of the RPE.

The association between low expression level of p21 and elevated level of plk1 suggested a possible connection of cell cycle regulation to regeneration. It is proposed that the lack of check points during cell cycle due to the p21 knockout, the percentage

of G2/M population will increase. A high G2/M cell percentage is also a feature of regenerative tissues like liver. Unscheduled entering into S phase will cause the phenotype of enhanced proliferating (118). Overexpression of polo-like kinase-1 may create similar situation including the unscheduled entering into S-phase and accumulation of G2/M phase cells.

The distinct expression profile of different TGF-β family members provides an interesting index of types of tissue repairing. It is not easy to explain our result that TGF-β1, TGF-β2 and TGF-β3 were all found to be expressed in higher level in regenerative strain. One explanation might be that the high level of TGF-β3 may dominate the regenerative like situation. Possible experiment can be carried out by inhibiting the TGF-β1, TGF-β2 and/or over expressing TGF-β3 and check the RPE regeneration. A promising therapeutic approach can be developed if this works.

The investigation of the possible regeneration mechanisms on chapter five provide general hint of the role circulating stem cell and microenvironment played during the regeneration process. Though circulating stem cell may play a pivotal important role in the regeneration, as suggested by others (70), synergetic effect may exist between the circulating stem cell and micro-environment during regeneration process by the result that the cohort with both p21 K.O. bone marrow cell and host regenerated better than the cohorts with either one factor. It is not surprising since the regeneration is a complex process. The motivation and differentiation requires series of signals and cytokines(73).

Recent studies provide additional information on how enhanced RPE regeneration can occur. Similar conclusion were draw in a study of a mouse myocardial injury and recovery model, which indicate circulating stem cells may be superior in MRL/MpJ

mice(70). Alternatively, the peripheral region of the posterior eye, which has been suggested to contain stem or progenitor cells (109), may be more proliferative in MRL/MpJ mice than in AKR/J mice. Finally, a less destructive inflammatory response in MRL/MpJ mice (119, 120) may promote the engraftment and regeneration of RPE cells or the proliferation of other tissue-derived cells. Studies in MRL/MpJ mice and other animal models have indicated that the status of systemic inflammatory factors and the local balance of pro- and anti-inflammatory cytokines profile are critical in determining whether a wound heals with or without a scar (120-123). Whichever hypothesis proves correct, if the mechanism of enhanced RPE regeneration in the MRL/MpJ mice can be clarified, it will be useful for developing therapies for clinical recovery from RPE damage and loss. The simple fact that RPE regeneration occurs robustly in MRL/MpJ mice may help efforts to identify the cell sources that effect RPE repair in a mammalian system. Studies from our own and other laboratories have shown that HSC derived donor cells can form cells within the RPE layer that are morphologically indistinguishable from native RPE (51-56). However, only low levels of donor cell incorporation were observed and it was challenging to confirm that these cells were fully functional. The extensive RPE regeneration in our wound healing mouse model may permit more robust incorporation of donor cells and facilitate functional testing of these populations within the RPE layer.

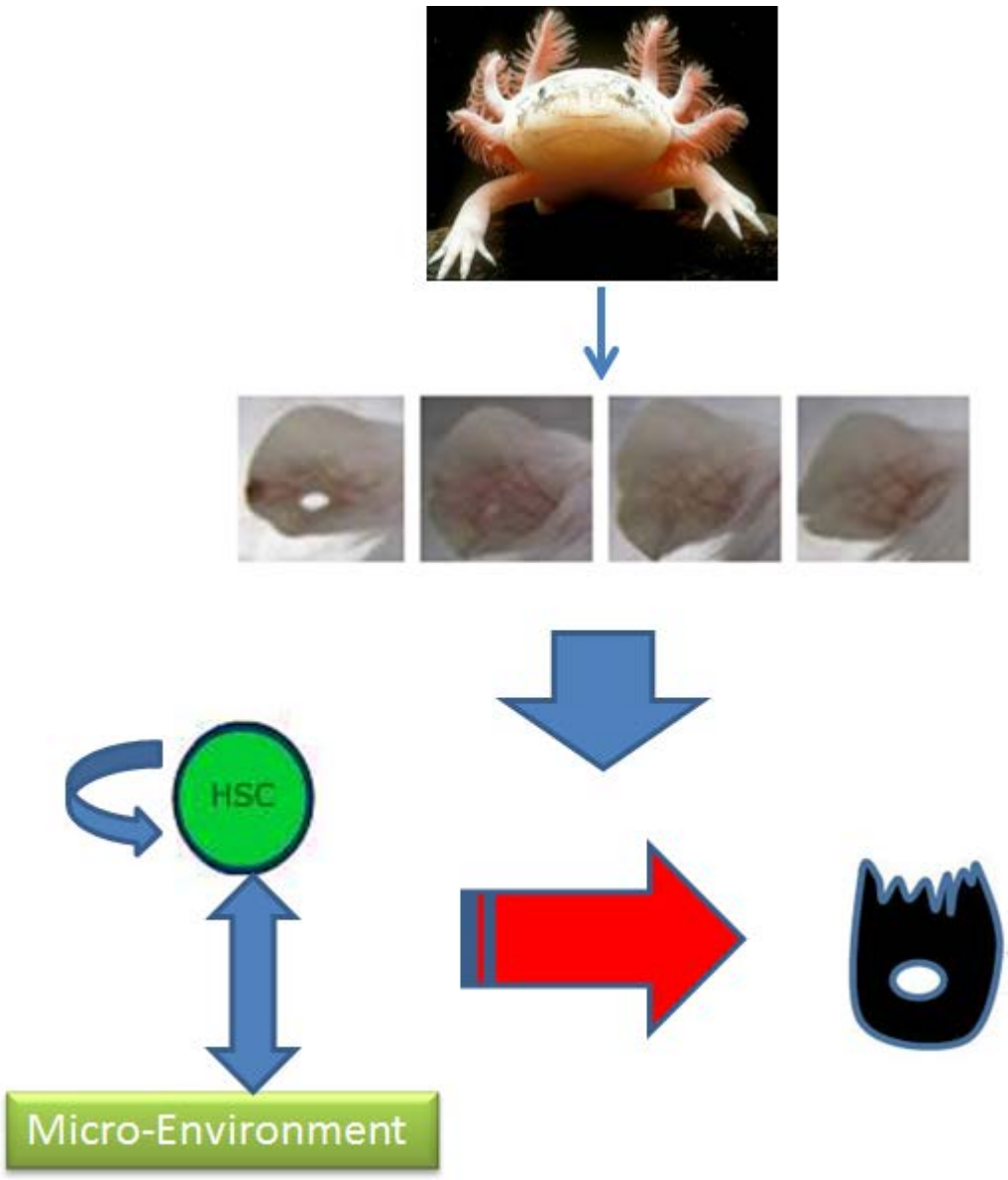

Figure 6-1. A schematic diagram that suggests the stem cell, micro-enviroment and the interactions that may contribute to RPE regeneration.

LIST OF REFERENCES

1. Kanda, A., Abecasis, G., and Swaroop, A. 2008. Inflammation in the pathogenesis of age-related macular degeneration. *Br J Ophthalmol* 92:448-450.

2. Rein, D.B., Wittenborn, J.S., Zhang, X., Honeycutt, A.A., Lesesne, S.B., and Saaddine, J. 2009. Forecasting age-related macular degeneration through the year 2050: the potential impact of new treatments. *Arch Ophthalmol* 127:533-540.

3. Klein, R., Klein, B.E., Jensen, S.C., and Meuer, S.M. 1997. The five-year incidence and progression of age-related maculopathy: the Beaver Dam Eye Study. *Ophthalmology* 104:7-21.

4. Mitchell, P., Wang, J.J., Foran, S., and Smith, W. 2002. Five-year incidence of age-related maculopathy lesions: the Blue Mountains Eye Study. *Ophthalmology* 109:1092-1097.

5. Mukesh, B.N., Dimitrov, P.N., Leikin, S., Wang, J.J., Mitchell, P., McCarty, C.A., and Taylor, H.R. 2004. Five-year incidence of age-related maculopathy: the Visual Impairment Project. *Ophthalmology* 111:1176-1182.

6. Patel, M., and Chan, C.C. 2008. Immunopathological aspects of age-related macular degeneration. *Semin Immunopathol* 30:97-110.

7. Zarbin, M.A. 2004. Current concepts in the pathogenesis of age-related macular degeneration. *Arch Ophthalmol* 122:598-614.

8. Swaroop, A., Chew, E.Y., Rickman, C.B., and Abecasis, G.R. 2009. Unraveling a multifactorial late-onset disease: from genetic susceptibility to disease mechanisms for age-related macular degeneration. *Annu Rev Genomics Hum Genet* 10:19-43.

9. Isas, J.M., Luibl, V., Johnson, L.V., Kayed, R., Wetzel, R., Glabe, C.G., Langen, R., and Chen, J. 2009. Drusen deposits contain soluble and mature amyloid fibrils. *Invest Ophthalmol Vis Sci*.

10. Malek, G., Johnson, L.V., Mace, B.E., Saloupis, P., Schmechel, D.E., Rickman, D.W., Toth, C.A., Sullivan, P.M., and Bowes Rickman, C. 2005. Apolipoprotein E allele-dependent pathogenesis: a model for age-related retinal degeneration. *Proc Natl Acad Sci U S A* 102:11900-11905.

11. Rizzolo, L.J. 2007. Development and role of tight junctions in the retinal pigment epithelium. *Int Rev Cytol* 258:195-234.

12. Strauss, O. 2005. The retinal pigment epithelium in visual function. *Physiol Rev* 85:845-881.

13. Al-Hussaini, H., Kam, J.H., Vugler, A., Semo, M., and Jeffery, G. 2008. Mature retinal pigment epithelium cells are retained in the cell cycle and proliferate in vivo. *Mol Vis* 14:1784-1791.

14. Zanke, B., Hawken, S., Carter, R., and Chow, D. 2010. A genetic approach to stratification of risk for age-related macular degeneration. *Can J Ophthalmol* 45:22-27.

15. Yildirim, Z., Ucgun, N.I., and Yildirim, F. 2011. The role of oxidative stress and antioxidants in the pathogenesis of age-related macular degeneration. *Clinics (Sao Paulo)* 66:743-746.

16. Beatty, S., Koh, H., Phil, M., Henson, D., and Boulton, M. 2000. The role of oxidative stress in the pathogenesis of age-related macular degeneration. *Surv Ophthalmol* 45:115-134.

17. Dong, A., Xie, B., Shen, J., Yoshida, T., Yokoi, K., Hackett, S.F., and Campochiaro, P.A. 2009. Oxidative stress promotes ocular neovascularization. *J Cell Physiol* 219:544-552.

18. Trevithick, J., Massel, D., Robertson, J.M., Tomany, S., and Wall, R. 2004. Model study of AREDS antioxidant supplementation of AMD compared to Visudyne: a dominant strategy? *Ophthalmic Epidemiol* 11:337-346.

19. Qi, X., Sun, L., Lewin, A.S., Hauswirth, W.W., and Guy, J. 2007. Long-term suppression of neurodegeneration in chronic experimental optic neuritis: antioxidant gene therapy. *Invest Ophthalmol Vis Sci* 48:5360-5370.

20. Chen, B., Caballero, S., Seo, S., Grant, M.B., and Lewin, A.S. 2009. Delivery of antioxidant enzyme genes to protect against ischemia/reperfusion-induced injury to retinal microvasculature. *Invest Ophthalmol Vis Sci* 50:5587-5595.

21. Sparrow, J.R. 2010. Bisretinoids of RPE lipofuscin: trigger for complement activation in age-related macular degeneration. *Adv Exp Med Biol* 703:63-74.

22. 2009. Deal watch: Alcon licenses complement pathway inhibitor for macular degeneration. *Nat Rev Drug Discov* 8:922.

23. 1991. Laser photocoagulation of subfoveal recurrent neovascular lesions in age-related macular degeneration. Results of a randomized clinical trial. Macular Photocoagulation Study Group. *Arch Ophthalmol* 109:1232-1241.

24. 1991. Subfoveal neovascular lesions in age-related macular degeneration. Guidelines for evaluation and treatment in the macular photocoagulation study. Macular Photocoagulation Study Group. *Arch Ophthalmol* 109:1242-1257.

25. Shah, A.M., Bressler, N.M., and Jampol, L.M. 2011. Does laser still have a role in the management of retinal vascular and neovascular diseases? *Am J Ophthalmol* 152:332-339 e331.

26. Zampros, I., Praidou, A., Brazitikos, P., Ekonomidis, P., and Androudi, S. 2012. Antivascular endothelial growth factor agents for neovascular age-related macular degeneration. *J Ophthalmol* 2012:319728.

27. Ciulla, T.A., and Rosenfeld, P.J. 2009. Antivascular endothelial growth factor therapy for neovascular age-related macular degeneration. *Curr Opin Ophthalmol* 20:158-165.

28. Singerman, L. 2009. Combination therapy using the small interfering RNA bevasiranib. *Retina* 29:S49-50.

29. Elbarbary, R.A., Takaku, H., Tamura, M., and Nashimoto, M. 2009. Inhibition of vascular endothelial growth factor expression by TRUE gene silencing. *Biochem Biophys Res Commun* 379:924-927.

30. Pechan, P., Rubin, H., Lukason, M., Ardinger, J., DuFresne, E., Hauswirth, W.W., Wadsworth, S.C., and Scaria, A. 2009. Novel anti-VEGF chimeric molecules delivered by AAV vectors for inhibition of retinal neovascularization. *Gene Ther* 16:10-16.

31. Bressler, N.M., Bressler, S.B., Childs, A.L., Haller, J.A., Hawkins, B.S., Lewis, H., MacCumber, M.W., Marsh, M.J., Redford, M., Sternberg, P., Jr., et al. 2004. Surgery for hemorrhagic choroidal neovascular lesions of age-related macular degeneration: ophthalmic findings: SST report no. 13. *Ophthalmology* 111:1993-2006.

32. Hillenkamp, J., Surguch, V., Framme, C., Gabel, V.P., and Sachs, H.G. 2010. Management of submacular hemorrhage with intravitreal versus subretinal injection of recombinant tissue plasminogen activator. *Graefes Arch Clin Exp Ophthalmol* 248:5-11.

33. Hillenkamp, J., Surguch, V., Framme, C., Gabel, V.P., and Sachs, H.G. 2012. Management of submacular hemorrhage with intravitreal versus subretinal injection of recombinant tissue plasminogen activator. *Graefes Arch Clin Exp Ophthalmol* 248:5-11.

34. Gurtner, G.C., Callaghan, M.J., and Longaker, M.T. 2007. Progress and potential for regenerative medicine. *Annu Rev Med* 58:299-312.

35. Nacu, E., and Tanaka, E.M. 2011. Limb regeneration: a new development? *Annu Rev Cell Dev Biol* 27:409-440.

36. Chernoff, E.A., Stocum, D.L., Nye, H.L., and Cameron, J.A. 2003. Urodele spinal cord regeneration and related processes. *Dev Dyn* 226:295-307.

37. Del Rio-Tsonis, K., and Tsonis, P.A. 2003. Eye regeneration at the molecular age. *Dev Dyn* 226:211-224.

38. Dawley, E.M., S, O.S., Woodard, K.T., and Matthias, K.A. 2012. Spinal cord regeneration in a tail autotomizing urodele. *J Morphol* 273:211-225.

39. Poss, K.D., Wilson, L.G., and Keating, M.T. 2002. Heart regeneration in zebrafish. *Science* 298:2188-2190.

40. Rossi, L., Challen, G.A., Sirin, O., Lin, K.K., and Goodell, M.A. 2011. Hematopoietic stem cell characterization and isolation. *Methods Mol Biol* 750:47-59.

41. Kierdorf, U., and Kierdorf, H. 2012. Antler regrowth as a form of epimorphic regeneration in vertebrates - a comparative view. *Front Biosci (Elite Ed)* 4:1606-1624.

42. Michalopoulos, G.K. 2007. Liver regeneration. *J Cell Physiol* 213:286-300.

43. Hongbo, S., Yu, C., Ming, K., Honglin, S., Yuanping, H., and Zhongping, D. 2012. Augmenter of Liver Regeneration may be a Candidate for Prognosis of HBV Related Acute-on-Chronic Liver Failure as a Regenerative Marker. *Hepatogastroenterology* 59.

44. Fernando, W.A., Leininger, E., Simkin, J., Li, N., Malcom, C.A., Sathyamoorthi, S., Han, M., and Muneoka, K. 2011. Wound healing and blastema formation in regenerating digit tips of adult mice. *Dev Biol* 350:301-310.

45. Okano, H. 2011. Strategic approaches to regeneration of a damaged central nervous system. *Cornea* 30 Suppl 1:S15-18.

46. Penn, M.S., Dong, F., Klein, S., and Mayorga, M.E. 2011. Stem cells for myocardial regeneration. *Clin Pharmacol Ther* 90:499-501.

47. Guan, X., Furth, M.E., and Childers, M.K. 2011. Stem cell use in musculoskeletal disorders. *Pm R* 3:S95-99.

48. Seagle, B.L., Gasyna, E.M., Mieler, W.F., and Norris, J.R., Jr. 2006. Photoprotection of human retinal pigment epithelium cells against blue light-induced apoptosis by melanin free radicals from Sepia officinalis. *Proc Natl Acad Sci U S A* 103:16644-16648.

49. Boulton, M., Roanowska, M., and Wess, T. 2004. Ageing of the retinal pigment epithelium: implications for transplantation. *Graefes Arch Clin Exp Ophthalmol* 242:76-84.

50. Lee, E., and Maclaren, R.E. 2010. Sources of RPE for replacement therapy. *Br J Ophthalmol*.

51. Harris, J.R., Brown, G.A., Jorgensen, M., Kaushal, S., Ellis, E.A., Grant, M.B., and Scott, E.W. 2006. Bone marrow-derived cells home to and regenerate retinal pigment epithelium after injury. *Invest Ophthalmol Vis Sci* 47:2108-2113.

52. Vossmerbaeumer, U., Kuehl, S., Kern, S., Kluter, H., Jonas, J.B., and Bieback, K. 2008. Induction of retinal pigment epithelium properties in ciliary margin progenitor cells. *Clin Experiment Ophthalmol* 36:358-366.

53. Carr, A.J., Vugler, A.A., Hikita, S.T., Lawrence, J.M., Gias, C., Chen, L.L., Buchholz, D.E., Ahmado, A., Semo, M., Smart, M.J., et al. 2009. Protective effects of human iPS-derived retinal pigment epithelium cell transplantation in the retinal dystrophic rat. *PLoS One* 4:e8152.

54. Harris, J.R., Fisher, R., Jorgensen, M., Kaushal, S., and Scott, E.W. 2009. CD133 progenitor cells from the bone marrow contribute to retinal pigment epithelium repair. *Stem Cells* 27:457-466.

55. Idelson, M., Alper, R., Obolensky, A., Ben-Shushan, E., Hemo, I., Yachimovich-Cohen, N., Khaner, H., Smith, Y., Wiser, O., Gropp, M., et al. 2009. Directed differentiation of human embryonic stem cells into functional retinal pigment epithelium cells. *Cell Stem Cell* 5:396-408.

56. Uygun, B.E., Sharma, N., and Yarmush, M. 2009. Retinal pigment epithelium differentiation of stem cells: current status and challenges. *Crit Rev Biomed Eng* 37:355-375.

57. Xu, Y., Shi, Y., and Ding, S. 2008. A chemical approach to stem-cell biology and regenerative medicine. *Nature* 453:338-344.

58. Metcalfe, A.D., and Ferguson, M.W. 2007. Tissue engineering of replacement skin: the crossroads of biomaterials, wound healing, embryonic development, stem cells and regeneration. *J R Soc Interface* 4:413-437.

59. Wicker, J., and Kamler, K. 2009. Current concepts in limb regeneration: a hand surgeon's perspective. *Ann N Y Acad Sci* 1172:95-109.

60. Shah, M., Foreman, D.M., and Ferguson, M.W. 1994. Neutralising antibody to TGF-beta 1,2 reduces cutaneous scarring in adult rodents. *J Cell Sci* 107 (Pt 5):1137-1157.

61. Shah, M., Foreman, D.M., and Ferguson, M.W. 1995. Neutralisation of TGF-beta 1 and TGF-beta 2 or exogenous addition of TGF-beta 3 to cutaneous rat wounds reduces scarring. *J Cell Sci* 108 (Pt 3):985-1002.

62. Ho, D.M., and Whitman, M. 2008. TGF-beta signaling is required for multiple processes during Xenopus tail regeneration. *Dev Biol* 315:203-216.

63. Levesque, M., Gatien, S., Finnson, K., Desmeules, S., Villiard, E., Pilote, M., Philip, A., and Roy, S. 2007. Transforming growth factor: beta signaling is essential for limb regeneration in axolotls. *PLoS One* 2:e1227.

64. Heber-Katz, E., Leferovich, J., Bedelbaeva, K., Gourevitch, D., and Clark, L. 2004. The scarless heart and the MRL mouse. *Philos Trans R Soc Lond B Biol Sci* 359:785-793.

65. Leferovich, J.M., Bedelbaeva, K., Samulewicz, S., Zhang, X.M., Zwas, D., Lankford, E.B., and Heber-Katz, E. 2001. Heart regeneration in adult MRL mice. *Proc Natl Acad Sci U S A* 98:9830-9835.

66. Ueno, M., Lyons, B.L., Burzenski, L.M., Gott, B., Shaffer, D.J., Roopenian, D.C., and Shultz, L.D. 2005. Accelerated wound healing of alkali-burned corneas in MRL mice is associated with a reduced inflammatory signature. *Invest Ophthalmol Vis Sci* 46:4097-4106.

67. Fitzgerald, J., Rich, C., Burkhardt, D., Allen, J., Herzka, A.S., and Little, C.B. 2008. Evidence for articular cartilage regeneration in MRL/MpJ mice. *Osteoarthritis Cartilage* 16:1319-1326.

68. Kostyk, S.K., Popovich, P.G., Stokes, B.T., Wei, P., and Jakeman, L.B. 2008. Robust axonal growth and a blunted macrophage response are associated with impaired functional recovery after spinal cord injury in the MRL/MpJ mouse. *Neuroscience* 156:498-514.

69. Masinde, G.L., Li, X., Gu, W., Davidson, H., Mohan, S., and Baylink, D.J. 2001. Identification of wound healing/regeneration quantitative trait loci (QTL) at multiple time points that explain seventy percent of variance in (MRL/MpJ and SJL/J) mice F2 population. *Genome Res* 11:2027-2033.

70. Alfaro, M.P., Pagni, M., Vincent, A., Atkinson, J., Hill, M.F., Cates, J., Davidson, J.M., Rottman, J., Lee, E., and Young, P.P. 2008. The Wnt modulator sFRP2 enhances mesenchymal stem cell engraftment, granulation tissue formation and myocardial repair. *Proc Natl Acad Sci U S A* 105:18366-18371.

71. Naviaux, R.K., Le, T.P., Bedelbaeva, K., Leferovich, J., Gourevitch, D., Sachadyn, P., Zhang, X.M., Clark, L., and Heber-Katz, E. 2009. Retained features of embryonic metabolism in the adult MRL mouse. *Mol Genet Metab* 96:133-144.

72. Caldwell, R.L., Opalenik, S.R., Davidson, J.M., Caprioli, R.M., and Nanney, L.B. 2008. Tissue profiling MALDI mass spectrometry reveals prominent calcium-binding proteins in the proteome of regenerative MRL mouse wounds. *Wound Repair Regen* 16:442-449.

73. Blank, U., Karlsson, G., and Karlsson, S. 2008. Signaling pathways governing stem-cell fate. *Blood* 111:492-503.

74. Grove, J.E., Bruscia, E., and Krause, D.S. 2004. Plasticity of bone marrow-derived stem cells. *Stem Cells* 22:487-500.

75. Tuch, B.E. 2006. Stem cells--a clinical update. *Aust Fam Physician* 35:719-721.

76. Luo, J., Chen, J., Deng, Z.L., Luo, X., Song, W.X., Sharff, K.A., Tang, N., Haydon, R.C., Luu, H.H., and He, T.C. 2007. Wnt signaling and human diseases: what are the therapeutic implications? *Lab Invest* 87:97-103.

77. Borggrefe, T., and Oswald, F. 2009. The Notch signaling pathway: transcriptional regulation at Notch target genes. *Cell Mol Life Sci* 66:1631-1646.

78. Watabe, T., and Miyazono, K. 2009. Roles of TGF-beta family signaling in stem cell renewal and differentiation. *Cell Res* 19:103-115.

79. Seuntjens, E., Umans, L., Zwijsen, A., Sampaolesi, M., Verfaillie, C.M., and Huylebroeck, D. 2009. Transforming Growth Factor type beta and Smad family signaling in stem cell function. *Cytokine Growth Factor Rev*.

80. Barr, F.A., Sillje, H.H., and Nigg, E.A. 2004. Polo-like kinases and the orchestration of cell division. *Nat Rev Mol Cell Biol* 5:429-440.

81. McInnes, C., and Wyatt, M.D. 2011. PLK1 as an oncology target: current status and future potential. *Drug Discov Today* 16:619-625.

82. Jopling, C., Sleep, E., Raya, M., Marti, M., Raya, A., and Izpisua Belmonte, J.C. 2010. Zebrafish heart regeneration occurs by cardiomyocyte dedifferentiation and proliferation. *Nature* 464:606-609.

83. Yardeni, T., Eckhaus, M., Morris, H.D., Huizing, M., and Hoogstraten-Miller, S. 2011. Retro-orbital injections in mice. *Lab Anim (NY)* 40:155-160.

84. Xia, H., Krebs, M.P., Kaushal, S., and Scott, E.W. 2011. Enhanced retinal pigment epithelium regeneration after injury in MRL/MpJ mice. *Exp Eye Res* 93:862-872.

85. Thevenaz, P., and Unser, M. 2007. User-friendly semiautomated assembly of accurate image mosaics in microscopy. *Microsc Res Tech* 70:135-146.

86. Li, Q., Timmers, A.M., Hunter, K., Gonzalez-Pola, C., Lewin, A.S., Reitze, D.H., and Hauswirth, W.W. 2001. Noninvasive imaging by optical coherence tomography to monitor retinal degeneration in the mouse. *Invest Ophthalmol Vis Sci* 42:2981-2989.

87. Ralph, G.S., Binley, K., Wong, L.F., Azzouz, M., and Mazarakis, N.D. 2006. Gene therapy for neurodegenerative and ocular diseases using lentiviral vectors. *Clin Sci (Lond)* 110:37-46.

88. Menger, B., Vogt, P.M., Kuhbier, J.W., and Reimers, K. 2010. Applying amphibian limb regeneration to human wound healing: a review. *Ann Plast Surg* 65:504-510.

89. Redfern, W.S., Storey, S., Tse, K., Hussain, Q., Maung, K.P., Valentin, J.P., Ahmed, G., Bigley, A., Heathcote, D., and McKay, J.S. 2011. Evaluation of a convenient method of assessing rodent visual function in safety pharmacology studies: effects of sodium iodate on visual acuity and retinal morphology in albino and pigmented rats and mice. *J Pharmacol Toxicol Methods* 63:102-114.

90. Hamel, C.P., Tsilou, E., Pfeffer, B.A., Hooks, J.J., Detrick, B., and Redmond, T.M. 1993. Molecular cloning and expression of RPE65, a novel retinal pigment epithelium-specific microsomal protein that is post-transcriptionally regulated in vitro. *J Biol Chem* 268:15751-15757.

91. Douglas, H.E. 2010. TGF-ss in wound healing: a review. *J Wound Care* 19:403-406.

92. Enzmann, V., Yolcu, E., Kaplan, H.J., and Ildstad, S.T. 2009. Stem cells as tools in regenerative therapy for retinal degeneration. *Arch Ophthalmol* 127:563-571.

93. Mizota, A., and Adachi-Usami, E. 1997. Functional recovery of retina after sodium iodate injection in mice. *Vision Res* 37:1859-1865.

94. Enzmann, V., Row, B.W., Yamauchi, Y., Kheirandish, L., Gozal, D., Kaplan, H.J., and McCall, M.A. 2006. Behavioral and anatomical abnormalities in a sodium iodate-induced model of retinal pigment epithelium degeneration. *Exp Eye Res* 82:441-448.

95. Machalinska, A., Lubinski, W., Klos, P., Kawa, M., Baumert, B., Penkala, K., Grzegrzolka, R., Karczewicz, D., Wiszniewska, B., and Machalinski, B. 2011. Sodium iodate selectively injuries the posterior pole of the retina in a dose-dependent manner: morphological and electrophysiological study. *Neurochem Res* 35:1819-1827.

96. Longbottom, R., Fruttiger, M., Douglas, R.H., Martinez-Barbera, J.P., Greenwood, J., and Moss, S.E. 2009. Genetic ablation of retinal pigment epithelial cells reveals the adaptive response of the epithelium and impact on photoreceptors. *Proc Natl Acad Sci U S A* 106:18728-18733.

97. Chadwick, R.B., Bu, L., Yu, H., Hu, Y., Wergedal, J.E., Mohan, S., and Baylink, D.J. 2007. Digit tip regrowth and differential gene expression in MRL/Mpj, DBA/2, and C57BL/6 mice. *Wound Repair Regen* 15:275-284.

98. Gourevitch, D.L., Clark, L., Bedelbaeva, K., Leferovich, J., and Heber-Katz, E. 2009. Dynamic changes after murine digit amputation: the MRL mouse digit shows waves of tissue remodeling, growth, and apoptosis. *Wound Repair Regen* 17:447-455.

99. Tolba, R.H., Schildberg, F.A., Decker, D., Abdullah, Z., Buttner, R., Minor, T., and von Ruecker, A. 2010. Mechanisms of improved wound healing in Murphy Roths Large (MRL) mice after skin transplantation. *Wound Repair Regen* 18:662-670.

100. Naseem, R.H., Meeson, A.P., Michael Dimaio, J., White, M.D., Kallhoff, J., Humphries, C., Goetsch, S.C., De Windt, L.J., Williams, M.A., Garry, M.G., et al. 2007. Reparative myocardial mechanisms in adult C57BL/6 and MRL mice following injury. *Physiol Genomics* 30:44-52.

101. Cimini, M., Fazel, S., Fujii, H., Zhou, S., Tang, G., Weisel, R.D., and Li, R.K. 2008. The MRL mouse heart does not recover ventricular function after a myocardial infarction. *Cardiovasc Pathol* 17:32-39.

102. Grisel, P., Meinhardt, A., Lehr, H.A., Kappenberger, L., Barrandon, Y., and Vassalli, G. 2008. The MRL mouse repairs both cryogenic and ischemic myocardial infarcts with scar. *Cardiovasc Pathol* 17:14-22.

103. Robey, T.E., and Murry, C.E. 2008. Absence of regeneration in the MRL/MpJ mouse heart following infarction or cryoinjury. *Cardiovasc Pathol* 17:6-13.

104. Davis, T.A., Amare, M., Naik, S., Kovalchuk, A.L., and Tadaki, D. 2007. Differential cutaneous wound healing in thermally injured MRL/MPJ mice. *Wound Repair Regen* 15:577-588.

105. Abdullah, I., Lepore, J.J., Epstein, J.A., Parmacek, M.S., and Gruber, P.J. 2005. MRL mice fail to heal the heart in response to ischemia-reperfusion injury. *Wound Repair Regen* 13:205-208.

106. Oh, Y.S., Thomson, L.E., Fishbein, M.C., Berman, D.S., Sharifi, B., and Chen, P.S. 2004. Scar formation after ischemic myocardial injury in MRL mice. *Cardiovasc Pathol* 13:203-206.

107. Korte, G.E., Perlman, J.I., and Pollack, A. 1994. Regeneration of mammalian retinal pigment epithelium. *Int Rev Cytol* 152:223-263.

108. Ringvold, A., Olsen, E.G., and Flage, T. 1981. Transient breakdown of the retinal pigment epithelium diffusion barrier after sodium iodate: a fluorescein angiographic and morphological study in the rabbit. *Experimental Eye Research* 33:361-369.

109. von Leithner, P.L., Ciurtin, C., and Jeffery, G. 2010. Microscopic mammalian retinal pigment epithelium lesions induce widespread proliferation with differences in magnitude between center and periphery. *Mol Vis* 16:570-581.

110. Nagai, H., and Kalnins, V.I. 1996. Normally occurring loss of single cells and repair of resulting defects in retinal pigment epithelium in situ. *Exp Eye Res* 62:55-61.

111. Florian, P., Schoneberg, T., Schulzke, J.D., Fromm, M., and Gitter, A.H. 2002. Single-cell epithelial defects close rapidly by an actinomyosin purse string mechanism with functional tight junctions. *J Physiol* 545:485-499.

112. Rosenblatt, J., Raff, M.C., and Cramer, L.P. 2001. An epithelial cell destined for apoptosis signals its neighbors to extrude it by an actin- and myosin-dependent mechanism. *Curr Biol* 11:1847-1857.

113. Kiuchi, K., Yoshizawa, K., Shikata, N., Moriguchi, K., and Tsubura, A. 2002. Morphologic characteristics of retinal degeneration induced by sodium iodate in mice. *Curr Eye Res* 25:373-379.

114. Korte, G.E., Mrowiec, E., Landzberg, K.S., and Youssri, A. 1995. Reorganization of actin microfilaments and microtubules in regenerating retinal pigment epithelium. *Exp Eye Res* 61:189-203.

115. Garcia-Fernandez, B., Campos, I., Geiger, J., Santos, A.C., and Jacinto, A. 2009. Epithelial resealing. *Int J Dev Biol* 53:1549-1556.

116. Reines, B., Cheng, L.I., and Matzinger, P. 2009. Unexpected regeneration in middle-aged mice. *Rejuvenation Res* 12:45-52.

117. Costa, R.A., Ruiz-de-Souza, V., Azevedo Jr, G.M., Vaz, N.M., and Carvalho, C.R. 2009. Effects of strain and age on ear wound healing and regeneration in mice. *Braz J Med Biol Res* 42:1143-1149.

118. Bedelbaeva, K., Snyder, A., Gourevitch, D., Clark, L., Zhang, X.M., Leferovich, J., Cheverud, J.M., Lieberman, P., and Heber-Katz, E. 2010. Lack of p21 expression links cell cycle control and appendage regeneration in mice. *Proc Natl Acad Sci U S A* 107:5845-5850.

119. Heber-Katz, E., and Gourevitch, D. 2009. The relationship between inflammation and regeneration in the MRL mouse: potential relevance for putative human regenerative(scarless wound healing) capacities? *Ann N Y Acad Sci* 1172:110-114.

120. Li, X., Mohan, S., Gu, W., and Baylink, D.J. 2001. Analysis of gene expression in the wound repair/regeneration process. *Mamm Genome* 12:52-59.

121. Anam, K., Amare, M., Naik, S., Szabo, K.A., and Davis, T.A. 2009. Severe tissue trauma triggers the autoimmune state systemic lupus erythematosus in the MRL/++ lupus-prone mouse. *Lupus* 18:318-331.

122. Eming, S.A., Hammerschmidt, M., Krieg, T., and Roers, A. 2009. Interrelation of immunity and tissue repair or regeneration. *Semin Cell Dev Biol* 20:517-527.

123. Zins, S.R., Amare, M.F., Anam, K., Elster, E.A., and Davis, T.A. 2010. Wound trauma mediated inflammatory signaling attenuates a tissue regenerative response in MRL/MpJ mice. *J Inflamm (Lond)* 7:25.

BIOGRAPHICAL SKETCH

Huiming Xia was born on 1981, in Lanxi, Zhejiang Province, China. He attended Nankai University on 2000 where he graduated first with bachelor's degree on life science and later with master's degree on microbiology. Huiming enrolled into the Interdisciplinary Program in Biomedical Sciences at the University of Florida in August of 2007 where he began his doctoral study under the guidance of Dr. Edward Scott in the Department of Molecular Genetics and Microbiology supported by Alumni Fellowship. After joining the laboratory of Dr. Edward Scott, Huiming began his research on investigating the regeneration of retinal pigment epithelium in the wound healing mice models. His scientific achievements include a first-author article published in Experimental Eye Research in October of 2011, a second-author article in Investigative Ophthalmology & Visual Science in November of 2011 and another first-author manuscript in preparation.